

Dynamical Tidal response of compact stars - An EFT approach

Gregory Jarequi,^a Soumodeep Mitra,^a and Varun Vaidya^a

^a*Department of Physics, University of South Dakota
Vermillion 57069, USA*

E-mail: Gregory.Jarequi@coyotes.usd.edu, Soumodeep.Mitra@coyotes.usd.edu,
Varun.Vaidya@usd.edu

ABSTRACT: We apply the point particle EFT approach to a compact star to systematically compute dynamical tidal love numbers for various non-rotating compact objects, extending the treatment of [1, 2]. We calculate the scattering amplitude in Black Hole Perturbation Theory (BPHT) for *arbitrary* non-rotating compact stars using the Mano-Suzuki-Takasugi (MST) method with non zero surface reflectivity and match it with that obtained from point particle EFT order by order in the low frequency expansion. This sets up a systematic framework for extracting the static and dynamical tidal love numbers (TLNs) to any order in the multipole expansion. In this paper, we employ the technique to compute the Next-to-Next-to Leading Order TLN upto a universal constant and its Renormalization Group equation for non-viscous Neutron stars and Neutron stars admixed with Bosonic or Fermionic dark matter.

Contents

1	Introduction	2
2	Point Particle EFT	4
2.1	The EFT action	4
2.2	Observable for matching to microscopic theory	5
2.3	The graviton scattering amplitude	6
2.4	Tail effect and RG running	7
3	Black hole Perturbation theory	10
3.1	Small frequency expansion	12
4	Solving stellar interior	13
4.1	Solution at $O(\omega^0)$	17
4.2	Solution at $O(\omega^1)$	18
4.3	Solution at $O(\omega^2)$	20
4.4	Surface reflectivity and compactness	21
5	Dynamical Tidal response from EFT matching	22
5.1	Neutron stars admixed with fermionic dark matter	22
5.2	Neutron Stars Admixed with Bosonic Dark Matter	27
6	Summary and Outlook	29
A	MST method for scattering amplitude	31
B	Additional results for TLNs	34

1 Introduction

Over the past decade the LIGO-VIRGO-KAGRA(LVK) [3–7] collaboration has detected gravitational waves (GW) from various compact object mergers, like black holes(BH) and neutron stars(NS). Such detections have provided us with a unique opportunity to test *strong-field* regime of general relativity(GR), cosmology, high density nuclear matter etc. [8–12] in a fundamentally new way. With various upcoming ground (e.g. Einstein Telescope [13]) and space based (e.g. LISA[14, 15]) detectors our capabilities of observing such events with improved accuracy and precision will increase significantly ushering in an era of precision gravitational wave astronomy. This will allow us to probe minute effects such as deviations from classical BH paradigm, imprint of astrophysical environments like dark matter (DM) as well as interior structure of compact objects such as NS.

The orbital dynamics and gravitational waveforms of binary systems depend sensitively on the internal structure of the stars which is described by equation of state (EoS). This equation characterizes how the density of matter that constitutes the star relates to its pressure. For the case of NS, the proposed theoretical models for EoS are diverse, with large uncertainty due to a lack of knowledge of how strongly interacting matter behaves at high densities. The situation becomes more complex when one considers NS immersed in some environment, like dark matter (DM), as is expected to happen in extreme mass ratio inspirals (EMRIs) around galactic supermassive BHs. In such cases, accretion of DM inside NS gives rise to DM admixed NS [16–19], which may significantly alter internal properties based on DM mass, cross-section between DM and nuclear matter, and other factors [20].

Knowledge of the EoS allows us to compute the NS tidal deformability, i.e. the tidal response of the star to an external gravitational field. This is described via a multi-pole expansion, the leading order of which is given by *static Tidal Love Numbers* (static TLNs), which measures the deformability of the object under time independent external tidal fields [21]. These have been studied extensively in literature and have the remarkable property that they vanished exactly for BHs in GR [22–24], but are non-zero for compact objects such as NS [25].

Static TLNs have been extensively used to probe the interior structure of NS. Greater tidal deformability results in a faster loss of orbital energy, which appears as a phase shift in the GW waveform. By determining how the NS EoS affects these TLNs, constraints on EOS have been imposed [20, 26]. In recent literature, investigation into TLN and subsequent constraints on various DM models using GW observation have been extended to the arena of other compact object e.g. DM admixed NS [27–31].

Although most studies on TLN, especially for NS and DM admixed NS systems (see [32–34] for some treatment of beyond static TLNs in NS) focus on the static regime, in recent years interest in higher order tidal responses has been growing steadily. This includes both time dependent tidal deformability given by *dynamical* TLN (dTLN) and tidal dissipation number (TDN), corresponding to the dissipative part of the tidal response which typically appear at higher order in the multipole expansion compared to the static TLN. This is because the effect of higher order dynamical tides increases during the late stage inspiral. In this region, with both compact objects near each other, the time dependence of external tidal field becomes important. Here, the time scale of internal tidal responses also becomes non-negligible in comparison to orbital

timescale as has been shown in [35, 36]. Further, [37] has shown that neglecting dynamical tides results in large biases in estimation of nuclear properties of NS. On the other hand, the dissipative part, i.e. TDN (which comes at next-to leading order in the multi-pole expansion of the tidal response function for NS) is related to the viscosity of the interior material and was found to be quite small [38]. However, in recent literature, authors have shown the effect of tidal dissipation in late-inspiral waveform to be quite important [39, 40].

As with NS, dynamical responses also become important for BHs and other compact objects (CO)s when modeling inspiral waveforms. While BHs in GR have vanishing static TLNs, the same is not true for dynamical TLNs (dTLN)[1, 41, 42]. Therefore, this should be taken into account to accurately model GW waveforms. Additionally, any modifications to a standard BH, such as compact objects, BH with environments, presence of higher dimensions, modification of asymptotically flat GR etc. is known to give rise to non-zero TLN [43–52]. Therefore, potential non-zero TLN observations, requiring precise GW waveform models, would signal physics beyond GR. Furthermore, non-zero BH TDNs can contribute to significant dephasing in EMRIs [53, 54]. This can be used to probe horizon-scale corrections originating from any underlying quantum gravity model [55, 56].

Calculation of dynamical tidal response is not without challenges and subtleties. In GR, the definition of TLN suffers from ambiguity due to coordinate dependent mixing of the external tidal field and the object’s response. In case of static TLNs such issues can be avoided using analytical continuation techniques, however this method cannot be extended for dynamical TLN [22, 57, 58]. Additionally, in recent literature[34, 59], authors have found an arbitrary convention dependent constant term entering at Next-to-Leading Order (dTLN). In practice such terms can introduce significant biases in the estimation of NS properties. These problems can be solved by using a worldline effective field theory (wEFT) or point particle EFT approach [60, 61] (see [62] for review), as has been recently shown by [1, 2, 63] in the case of rotating BH and non-rotating NS.

In this approach, one approximates the CO as a point particle at leading order, while the finite size effects are encoded via higher dimensional operators. Here the Wilsonian coefficients represent the tidal response of the object. These coefficients can then be obtained by matching some suitable observable calculated from both EFT and full theory GR. In [1], the authors have obtained the dynamical tidal response of a rotating BH in all order of spin up to Next-to-Next Leading order (NNLO) considering small frequency approximation. Whereas, in [2], the authors first used this technique to obtain leading order TLN and TDN for NS.

In this paper, we extend previous computations on static and dTLN for a class of COs. We first improve the result in [2] to NNLO, computing the static and lowest dynamical TLN for a NS with no viscosity (hence zero dissipation). We then expand the regime of the previous work to include DM admixed NS systems. Once again, we calculate up to NNLO and comment on the effect of various DM properties. We also explore the Renormalization Group evolution for these dTLNs.

The paper is structured as follows: In Section. 2 we recap the wEFT method, define the TLNs and TDNs and compute the graviton-CO scattering amplitude used as the observable for matching. In Section. 3 we calculate the same observable in full GR using MST formalism for a

CO with non-zero reflectivity. We then solve the interior solution of the compact object for NS and NS+DM system to derive the surface reflectivity of the star in terms of its interior properties in Section. 4. We use these results to match the scattering amplitude to the EFT result to derive the tidal responses of various compact objects in Section. 5 and present our conclusions in Section 6.

Throughout the paper we will use $c = 1$ units and mostly plus metric signature $(-, +, +, +)$. Greek indices denote components $0, \dots, 3$ and Latin indices will denote spacelike components.

2 Point Particle EFT

Let us first briefly describe the technique of obtaining the TLN with an EFT approach. In point particle or wEFT formalism, the CO when probed at a length scale r much larger than its size R , can be effectively treated as a point particle at leading order in the ratio r/R . The finite size effects, carrying information about the interior structure, can be incorporated via higher order terms through a multi-pole expansion. Static and dynamical TLN and TDN in this formalism can be defined as the Wilsonian coefficients of these higher order operators in a gauge invariant manner. However, to extract the values of the coefficients, one needs to do a matching of the EFT with the full UV-complete theory, namely black hole perturbation theory (BHPT). The matching can then be accomplished by comparing gauge-invariant observables calculated from EFT and BHPT, such as the scattering amplitude of a long wavelength GW impinging on the CO. To do this matching explicitly, we first calculate the scattering amplitude in both wEFT formalism and BHPT, then match them order by order in the expansion parameter $\epsilon = 2GM\omega$. Here ω is the frequency of the impinging wave and M the mass of the CO. For the case of NS or DM admixed NS systems, the scattering amplitude obtained from BHPT will contain information about the interior structure of the CO in terms of a surface reflectivity term, which we will explicitly obtain by solving Einstein's field equations in the interior of the CO.

2.1 The EFT action

We start with a brief review of the point particle EFT formalism for compact objects [60, 61]. At leading order, the dynamics is described by a massive point particle action coupled to gravity

$$S_{p.p} = -M \int d\tau = -M \int d\lambda \sqrt{-\frac{dx^\mu}{d\lambda} \frac{dx^\nu}{d\lambda} g_{\mu\nu}}, \quad (2.1)$$

where τ is the proper time and λ can be any monotonically increasing affine parameter. The leading finite size effects are introduced through higher dimensional operators that satisfy symmetry constraints, i.e. diffeomorphism and reparameterization invariance. In a vacuum background, the Ricci tensor is zero, hence the leading non-trivial object is the Weyl tensor, which is the traceless part of the Riemann tensor. For a particle without spin degrees of freedom, the only non-trivial tensor is the 4 velocity $u^\mu = dx^\mu/d\tau$. Hence the lowest order action beyond the point particle that couples the particle to gravity can be written as

$$S = S_{p.p} + \int d\tau \left[c_E E^{\mu\nu} E_{\mu\nu} + c_B B^{\mu\nu} B_{\mu\nu} \right] \quad (2.2)$$

where

$$E^{\mu\nu} = C^{\mu\rho\nu\sigma} u_\rho u_\sigma, \quad B^{\mu\nu} = (1/2) \epsilon_{\gamma(\mu}^{\alpha\beta} C_{\alpha\beta|\nu)\delta} u^\gamma u^\delta \quad (2.3)$$

with $C_{\mu\nu\rho\sigma}$ being the Weyl tensor. Note that the $E \cdot B$ type term is forbidden since in GR with a non-spinning point particle, parity is a good symmetry. For the case of a static particle with $u^\mu = (1, 0, 0, 0)$, given that the tidal fields $E^{\mu\nu}$, $B^{\mu\nu}$ are orthogonal to the 4-velocity, only their projection orthogonal to the direction of 4 velocity are relevant. Since $[E^2] = [B^2] = 4$, these operators are suppressed by $1/r^4$. Hence to define a dimensionless Wilson co-efficient, we can factor out terms which scale as the size of a black hole with mass M, namely $r_H \sim GM$

$$S = S_{p,p} - M(GM)^4 \int d\tau \left[\Lambda_E E^{ij} E_{ij} + \Lambda_B B^{ij} B_{ij} \right] \quad (2.4)$$

We can extend this action to account for higher order effects in two ways. First, taking higher order spatial derivatives¹ gives access to higher multiple moments and hence higher static TLNs. Secondly, higher order proper time derivatives will give *dynamical* TLNs. The action can then be written as

$$S = S_{p,p} - M(GM)^4 \sum_{n=0}^{\infty} \sum_{l=2}^{\infty} \int d\tau \left[(-1)^n (GM)^n \Lambda_{\omega^n}^{E,l} \frac{d^n \nabla^{i_3} \dots \nabla^{i_l} E^{ij}}{d\tau^n} \nabla_{i_3} \dots \nabla_{i_l} E_{ij} + E \leftrightarrow B \right] \quad (2.5)$$

Note that this series includes operators that are odd under time reversal, signifying irreversibility of dynamics, and hence encoding absorption/dissipation. Higher order operators with proper time derivatives are suppressed by the parameter $GM\omega$ which, along with R/r , forms another expansion parameter of our EFT. This indicates that in the EFT we do not excite any internal degrees of freedom of the star.

2.2 Observable for matching to microscopic theory

The Wilson coefficients $\Lambda_{\omega^n}^{E/B,l}$ can be obtained either by comparing the predictions of this EFT for a specific observable with data, or with the order by order expansion in $R/r, GM\omega$ of an explicit calculation if the microscopic theory is known. In this paper, we will do the latter. The observable chosen is the amplitude for scattering a low frequency ($GM\omega \ll 1$) graviton off our heavy static compact object of mass M

$$\begin{aligned} \text{out} \langle \mathbf{k}', h' | \mathbf{k}, h \rangle_{\text{in}} &\equiv \langle \mathbf{k}', h' | S | \mathbf{k}, h \rangle = \langle \mathbf{k}', h' | \mathbf{1} + iT | \mathbf{k}, h \rangle \\ &= 2\omega(2\pi)^3 \delta^3(\mathbf{k} - \mathbf{k}') \delta_{hh'} + 2\pi \delta(\omega - \omega') \times i\mathcal{M}(\omega, \mathbf{k} \rightarrow \mathbf{k}', h \rightarrow h') \end{aligned} \quad (2.6)$$

where \mathbf{k}, \mathbf{k}' are in the incoming and outgoing momenta of a graviton with helicity h and h' respectively. The scattering amplitude is proportional to $\delta(\omega - \omega')$ which conserves the energy of the graviton. This follows if we assume the 4 velocity u^μ to be independent of τ , which effectively is taking the limit $M \rightarrow \infty$. In principle, the four velocity also fluctuates and recoil effects are needed to accurately compute the scattering amplitude. But if we are only interested in the tidal

¹The projection along the ‘spatial’ direction is defined as $P^\mu_\nu = \delta^\mu_\nu + u^\mu u_\nu$

love numbers and dissipation numbers then we can ignore recoil in both the full theory and the effective theory, i.e. effectively take $M \rightarrow \infty$ (while keeping $GM\omega \ll 1$) before matching, which should suppress all recoil effects which will appear as powers of $1/M$. For the purpose of matching, we need the scattering amplitude in the spherical basis, which can be computed as

$$\mathcal{A}(\omega, l, m, h \rightarrow \omega, l', m', h') = \int \frac{d^3\mathbf{k}_1 d^3\mathbf{k}_2}{(2\pi)^6 \times 4|\mathbf{k}_1||\mathbf{k}_2|} \sum_{h_1, h_2} \langle \omega, l', m', h' | \mathbf{k}_2, h_2 \rangle \mathcal{M}(\omega, \mathbf{k}_1 \rightarrow \mathbf{k}_2, h_1 \rightarrow h_2) \langle \mathbf{k}_1, h_1 | \omega, l, m, h \rangle \quad (2.7)$$

The overlap of the plane wave with the spherical basis is given as

$$\langle \omega, l, m, h | \mathbf{k}, h \rangle = (2\pi)^2 \sqrt{\frac{2l+1}{2\pi\omega}} \delta(\omega - |\mathbf{k}|) \delta_{hh'} D_{mh}^l(\phi, \theta) \quad (2.8)$$

with

$$D_{mh}^l(\phi, \theta) = (-1)^m \sqrt{\frac{4\pi}{2l+1}} {}_h Y_{l,-m}(\phi, \theta) \quad (2.9)$$

where ${}_h Y_{l,-m}(\phi, \theta)$ are the spin weighted spherical harmonics. We see that the amplitude \mathcal{A} is dimensionless and can be related to the absorption probability and elastic scattering phase shift in the usual manner

$$i\mathcal{A} = 1 - \eta_{lm} e^{2i\delta_{lm}} \quad (2.10)$$

where $1 - \eta_{lm}^2$ is the absorption probability.

2.3 The graviton scattering amplitude

Using our action we can now compute the scattering amplitude $i\mathcal{M}$ order by order in perturbation theory. In the transverse traceless or radiation gauge, the tidal field at leading order in the metric perturbation $h_{\mu\nu}$ is simply $E_{ij}(x^\mu(\tau)) = -1/2\ddot{h}_{ij}(x^\mu(\tau))$. For a static object and using $\langle 0 | h_{ij}(\mathbf{x}) | \mathbf{k}, h \rangle = 1/M_{\text{pl}} \exp(-ik \cdot x) \epsilon_{ij}^h(\mathbf{k})$, we get

$$i\mathcal{M}^{(0)}(\mathbf{k}_{\text{in}} \rightarrow \mathbf{k}_{\text{out}}, h \rightarrow h') = -i \frac{\omega^4}{4M_{\text{pl}}^2} \Lambda^E \epsilon_h^{ij}(\mathbf{k}_{\text{in}}) \epsilon_{h'}^{*ij}(\mathbf{k}_{\text{out}}) M(GM)^4 + \text{magnetic} \quad (2.11)$$

which then allows us to write the amplitude in the spherical basis as

$$i\mathcal{A}^{(0)}(\omega, l = 2, m, h \rightarrow l = 2, m, h) = -i \frac{\omega^5}{40M_{\text{pl}}^2 \pi} M(GM)^4 \Lambda_{\omega^0}^E + \text{magnetic} \quad (2.12)$$

where $M_{\text{pl}} = \sqrt{\frac{\hbar}{32\pi G}}$. Confining ourselves to $l = 2$, but going to higher order in ω , we gain access

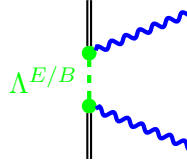
to the NLO tidal responses,

$$i\mathcal{A}^{(1)}(\omega, l = 2, m, h \rightarrow l = 2, m, h) = \frac{\omega^6}{40M_{\text{pl}}^2\pi} M(GM)^5 (H_{\omega_1}^E) + \text{magnetic} \quad (2.13)$$

where $\Lambda_{\omega_1}^E$ is the leading tidal dissipation number. In this paper, we go up to NNLO so we also need the next order which is simply

$$i\mathcal{A}^{(2)}(\omega, l = 2, m, h \rightarrow l = 2, m, h) = -i \frac{\omega^7}{40M_{\text{pl}}^2\pi} M(GM)^6 (\Lambda_{\omega_2}^E) + \text{magnetic} \quad (2.14)$$

Together the scattering amplitude with tidal operators is given by the following diagram,



$$\quad (2.15)$$

where, $\Lambda^{E/B}$ is a short hand for tidal operators up to NNLO order. The blue wavy lines represents incoming and outgoing gravitons, with the solid double lines represent the CO worldline. Writing the amplitude explicitly:

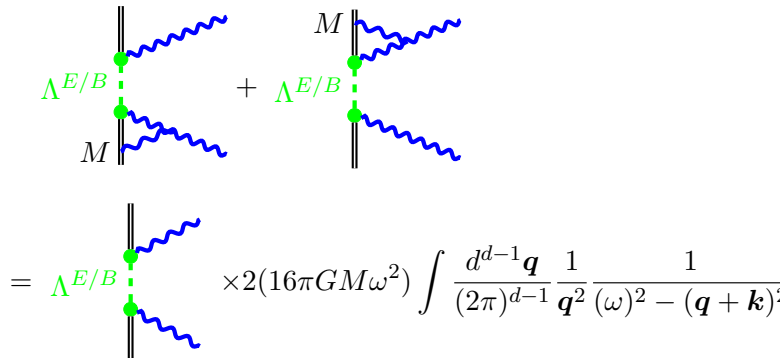
$$i\mathcal{A}_{0\text{PM}} = -i \frac{\omega^5}{40\pi M_{\text{pl}}^2} M(GM)^4 \mathcal{F}^E(\omega) + \text{magnetic} \quad (2.16)$$

Where we have defined the response function $\mathcal{F}^E(\omega) = \Lambda_{\omega_0}^E + i(GM\omega)H_{\omega_1}^E + (GM\omega)^2\Lambda_{\omega_2}^E$ and $H_{\omega_1}^E \equiv \Lambda_{\omega_1}^E$.

2.4 Tail effect and RG running

The results of previous section are however not complete, as we have neglected loop corrections from GR to the tidal operator insertions in the higher order scattering amplitude. We can incorporate these pieces as Post-Minkowskian (PM) corrections to the 0th order PM result shown above. Below we briefly describe the procedure and direct readers to [63–65] for further details.

Let us first consider the 1-PM correction to the scattering amplitude manifesting as 1-loop correction and given by the diagrams,



$$\quad (2.17)$$

2PM corrected response function

$$\mathcal{F}_{2\text{PM}}^E(\omega) = \mathcal{F}_r^E(\omega) \times \left(1 + 2GM\omega\pi - \frac{428}{105}(GM\omega)^2 \log\left(\frac{\omega}{\mu}\right) + (GM\omega)^2 \left[\frac{4\pi^2}{3} + \frac{634913}{44100} \right] \right) + (\text{magnetic}) \quad (2.22)$$

Where $\mathcal{F}_r^E(\omega)$ is given in terms of renormalized dTLN $\Lambda_{r,\omega^2}^E(\mu)$, with renormalization scale μ . We have denoted the logarithm appearing due to the 2-loop UV divergence with *violet* color, and in the BHPT section we will denote such terms in the same color for the purpose of easy identification. Since we require our observed scattering amplitude to be independent of the renormalization scale, this induces a running for the Λ_{ω^2} Wilson co-efficient as

$$\frac{\partial \Lambda_{r,\omega^2}^{E/B}(\mu)}{\partial \log(\mu)} = -\frac{428}{105} \Lambda_{\omega^0} \quad (2.23)$$

Finally, there is one another source of logarithmic divergence that we have not considered yet. The *violet* terms in the EFT arises are not universal, as they depend on the TLNs (such as Λ_{ω^0} in eqn. (2.23)) related to the object. On the other hand, GR non-linearities which arise from purely the point particle action can add correction terms, as shown in [1] in the case of BH. Such terms should be universal and we will show in that we recover these logarithms in the full theory(BHPT) NS case as well. On the EFT side, these terms appear at 6-loop order. The full computation of these 6-loop diagrams on EFT side is outside the scope of this paper, but we can infer the coefficient of this universal log term assuming consistency of our EFT from the BHPT matching². This allows us to write down the form of the log running including the universal piece as

$$\frac{\partial}{\partial \log(\mu)} \Lambda_{r,\omega^2}^E(\mu) = c - \frac{428}{105} \Lambda_{\omega^0} \quad (2.24)$$

The universal logarithmic terms will be denoted in *red* colored terms in the EFT and BHPT results. c for the universal logarithm can be read off by matching with BHPT, which in a later section will be shown to be $c = \frac{32}{45}$.

Pulling all the pieces together, we can finally write down the 2-PM corrected response function

$$\mathcal{F}_{2\text{PM}}^E(\omega) = \left\{ \Lambda_{\omega^0}^E + 2(GM\omega)\pi\Lambda_{\omega^0}^E + (GM\omega)^2 \left[\Lambda_{r,\omega^2}^E(\mu) - \frac{428}{105} \Lambda_{\omega^0}^E \log\left(\frac{\omega}{\mu}\right) + c \log\left(\frac{\omega}{\mu}\right) \right] \right. \quad (2.25)$$

$$\left. + \Lambda_{\omega^0}^E (GM\omega)^2 \left[\frac{4\pi^2}{3} + \frac{634913}{44100} \right] + \mathfrak{A}_{FZ} \right\} + i \left\{ (GM\omega)H_{\omega^1}^E + 2(GM\omega)^2 \pi H_{\omega^1}^E \right\}$$

The corrections in the EFT that lead to the universal logarithmic term in red can also contribute non-logarithmic finite pieces which are again universal. We include these pieces through \mathfrak{A}_{FZ} , which is a placeholder for all such contributions that we have not calculated here. These cannot be determined through consistency alone and a 6-loop calculation arising from the pure point

²Existence of the universal log term was predicted in [1], which was absent in the NS dTLN calculation of [33]. We show in our paper that such terms indeed exist in case of NS as well, providing strong evidence for the universal nature of these logs alluded to in [1].

particle action is needed to fix them, which is beyond the scope of this paper. Thus our final result for the TLN at this order is only correct up to an unknown constant which is universal in the sense that it does not depend on the internal properties of the star. The full 2-PM corrected scattering amplitude is given by

$$i\mathcal{A}_{2\text{PM}} = -i \frac{\omega^5}{40\pi M_{\text{pl}}^2} M(GM)^4 \mathcal{F}_{2\text{PM}}^E(\omega) + (\text{magnetic}) \quad (2.26)$$

We have used this result to match with BHPT scattering amplitude. Next we turn to the explicit calculation of this scattering amplitude in the full theory.

3 Black hole Perturbation theory

The problem of incoming wave of helicity h scattering off BH background is well studied (see [66] for review) and we will only briefly recap relevant parts here. For our purpose of deriving BHPT scattering amplitude results, we will employ the technique developed by Mano-Suzuki-Takasugi (MST method) [67–70]. This method matches quite well with the EFT approach, since in this method one can systematically obtain a low frequency expansion of the scattering amplitude, which is amenable for matching to the EFT. This is, as we saw in the previous sections, is also organized as a low frequency expansion.

The MST method can be used for general spin- s perturbation on a Kerr background, which for a GW (i.e. spin-2) perturbation, results in the Teukolsky equation. However, in this paper we will only work with non-rotating compact objects, and the resulting perturbation equation reduces to Regge-Wheeler(RW) equation [71] (using a Chandrasekhar transformation). We then solve this using the MST approach following [72] to obtain the scattering amplitude. The RW equation is given as

$$\left[\frac{d^2}{dr_*^2} + (\omega^2 - V(r)) \right] X_{\omega\ell}(r) = 0 \quad (3.1)$$

with $V(r)$ being defined as

$$V(r) = \left(1 - \frac{2M}{r} \right) \left[\frac{\ell(\ell+1)}{r^2} - \frac{6M}{r^3} \right] \quad (3.2)$$

Where the explicit definition of (radial) RW variable $X(r)$ is given in Appendix A. Furthermore, as our interest is in COs, we must use the reflective boundary condition at the surface of the object. Unlike a BH, any CO will reflect part of the incident wave back from its surface. This reflection depends on the interior properties of the object, and can either be calculated from solving the interior structure (e.g. for NS) or from first principles (e.g. Quantum corrected BH [73–75]). The reflection coefficient or reflectivity then carries the physical information about the constituents and thus can be used to put constraints on hereto unknown interior microstructure of these COs. We have explicitly shown the calculation in Appendix A and produce the final result for the scattering amplitude here.

In case of BH, i.e with purely ingoing boundary condition at horizon, the scattering amplitude

reads [72],

$$S_{BH} = \omega^{-2s} e^{-2i\epsilon l n \epsilon} \frac{A_{C,out}^\nu}{A_{C,in}^\nu} \left[\frac{1 + \beta_\nu \frac{K_{-\nu-1}}{K_\nu}}{1 + \alpha_\nu \frac{K_{-\nu-1}}{K_\nu}} \right] \quad (3.3)$$

The explicit forms of these functions are given in Appendix A.

However, for more general case of a compact object, which have a non-zero surface reflectivity, this amplitude gets modified to

$$S = \omega^{-2s} e^{-2i\epsilon l n \epsilon} \frac{A_{C,out}^\nu}{A_{C,in}^\nu} \left[\frac{1 + \beta_\nu \frac{K_{-\nu-1}}{K_\nu} \left(\frac{\mathfrak{B}_{-\nu-1}}{\mathfrak{B}_\nu} \right)}{1 + \alpha_\nu \frac{K_{-\nu-1}}{K_\nu} \left(\frac{\mathfrak{B}_{-\nu-1}}{\mathfrak{B}_\nu} \right)} \right]. \quad (3.4)$$

The ratio $\frac{\mathfrak{B}_{-\nu-1}}{\mathfrak{B}_\nu}$, is a function of the physical reflectivity at the surface of the object and can be defined in terms of interior properties of the NS (or NS+DM). We therefore relate it to the solution of the RW equation X in the interior of the star, following the technique employed in [2], by defining the matching parameter

$$T = \frac{r}{X} \frac{dX}{dr_*} \Big|_{r=R_s} \quad (3.5)$$

where R_s is the radius of the surface of the star. Furthermore, r_* is the tortoise co-ordinate given by $r_* = r + 2M \ln \left(\frac{r}{2M} - 1 \right)$. Equating the RHS of the equation for the interior and the exterior solution for X allows us to write

$$\frac{\mathfrak{B}_{-\nu-1}}{\mathfrak{B}_\nu} = \frac{TX^\nu - (r - 2M) \frac{dX^\nu}{dr}}{(r - 2M) \frac{dX^{-\nu-1}}{dr} - TX^{-\nu-1}} \quad (3.6)$$

which we can evaluate at the surface of the star $r = R_s$. Here we have used the solution for the RW variable written in terms of $X^\nu(r), X^{-\nu-1}(r)$ in the stellar exterior using (A.3) and (A.1). The matching parameter T can be obtained in terms of the interior properties of the star by solving the stellar perturbation equation for X in the stellar interior in the next section. We will then use this to compute eqn. (3.6) and hence the BHPT scattering amplitude. This can then be expanded order by order in ω to match to the EFT result.

Before we expand the scattering amplitude order by order in ϵ , another simplification follows from the "Near-Far factorization" of the scattering amplitude [1, 63, 76]. The reasoning of such factorization stems from the physical picture that any wave incident from infinity (in practice, far away from the body) suffers scattering from two sources- scattering due to the background potential, and scattering from the CO surface. Intuitively, one can see it is only the second scattering that contains the information about the tidal response. Further, one can also show, that the near and far zone scales as non-integer and integer powers of renormalized angular momentum ν respectively, barring a tail effect induced log term in far zone [1]. Therefore, in our work, following the past investigations of TLNs, we will only consider the near zone portion of

the scattering amplitude, given by

$$S_{NZ} = \frac{1 + \beta_\nu \frac{K_{-\nu-1}}{K_\nu} \left(\frac{\mathfrak{B}_{-\nu-1}}{\mathfrak{B}_\nu} \right)}{1 + \alpha_\nu \frac{K_{-\nu-1}}{K_\nu} \left(\frac{\mathfrak{B}_{-\nu-1}}{\mathfrak{B}_\nu} \right)}. \quad (3.7)$$

However, as demonstrated in [1, 77], this factorization is not without caveats. The main issue arises in the dTLNs, where the factorization technique along with the matching procedure can correctly recover the logarithmic pieces, but the non-log terms may get contributions from far zone. To correctly assess these terms, one needs to do a full expansion of the scattering amplitude and the corresponding matching, which we will produce in a forthcoming work.

3.1 Small frequency expansion

We are now in a position to undertake the small-frequency expansion of the near zone scattering amplitude. Here we follow the generic l prescription, as discussed before, however, which has its subtlety. In this case, taking the physical limit of $l \rightarrow n \in \mathbb{N}$ after the expansion at a particular order of ϵ gives poles at $l = n$ in far zone. In [77] authors have shown in case of $l = 1, s = 0$, such poles also appear in far zone and cancels out in the full scattering amplitude, making them nonphysical from an observables standpoint. While an explicit calculation for $s = -2, l = 2$ is not present, we assume the conjecture of [77] that such poles cancel out in full scattering amplitude for all l . Indeed for our case, we find such terms with poles in near-zone at ϵ^7 order of the form $-\frac{1}{225(l-2)}$, which we will not consider due to this. We can write the scattering amplitude as

$$S_{NZ} = 1 - \eta_{20} e^{2i\delta_{20}^{NZ}} \quad (3.8)$$

The small frequency expansion reads

$$\eta_{20} = 1 + S_1 \epsilon^6 + \pi S_1 \epsilon^7. \quad (3.9)$$

and

$$2\delta_{20}^{NZ} = S_0 \epsilon^5 + \pi S_0 \epsilon^6 + \left[S_2 - \left(\frac{107}{105} S_0 \log(\epsilon) + \frac{2}{225} \log(\epsilon) \right) \right] \epsilon^7 \quad (3.10)$$

where

$$S_0 = -\frac{2(6\mathcal{C} + T_0 - 3)}{75(6(\mathcal{C} - 1)\mathcal{C}(4\mathcal{C}^3 + 2\mathcal{C}^2 - 3) - 2\mathcal{C}(\mathcal{C}(6\mathcal{C}^2 + 4\mathcal{C} + 3) + 3)T_0 - 3\log(1 - 2\mathcal{C})(6\mathcal{C} + T_0 - 3))}$$

$$S_1 = -\frac{32\mathcal{C}^4 T_1}{25(-6(\mathcal{C} - 1)\mathcal{C}(4\mathcal{C}^3 + 2\mathcal{C}^2 - 3) + 2\mathcal{C}(\mathcal{C}(6\mathcal{C}^2 + 4\mathcal{C} + 3) + 3)T_0 + 3\log(1 - 2\mathcal{C})(6\mathcal{C} + T_0 - 3))^2} \quad (3.11)$$

Here we have expanded the matching quantity T as $T = T_0 - (iR\omega)T_1 - (R\omega)^2 T_2 + \dots$, and $\mathcal{C} = \frac{M}{R_s}$ denotes the compactness of the star. We have also not presented the full cumbersome expression of S_2 in the main text, the exact expression can be found in the accompanying Mathematica

notebook. We note here that the BHPT encodes the higher PM corrections (violet terms), the universal logarithmic pieces (red terms) and the tail effects (orange terms) that we observed in the EFT. We can now match BHPT results with EFT calculation to obtain the tidal love and dissipation numbers in terms of the CO properties, encoded in T and C . This will be done in Section 5.

In the next section we will now use stellar perturbation theory to explicitly calculate these two quantities T and C in terms of NS and NS+DM interior structure.

4 Solving stellar interior

To specify surface reflectivity of a compact object in terms of the properties of the star, we need to solve for the interior structure. Here we will consider the general treatment for a non-rotating CO, representing both NS and DM admixed NS system. We will treat matter within the NS as a viscous Landau fluid [78], specified by some equation of state. We will then solve the resulting Einstein's field equation due to the fluid stress energy tensor order by order in ω . In this paper, we will solve up to second order in ω , allowing us to access the NNLO dTLN.

It must be noted that at second order in ω , the Landau fluid model breaks down for viscous fluids and no longer guarantees a sub-luminal speed of sound in the fluid, therefore different fluid models such as the Israel-Stewart model must be used if we want to treat viscosity beyond NLO. In this paper, we only consider, Landau fluid model and therefore, for the calculation of ω^2 terms, we drop the viscosity from our model. Further, we wish to model dark matter as a non-viscous perfect fluid, to remain agnostic towards any particular model. However, in the following we will keep viscosity related terms in the calculation up until ω^6 order(NLO), to match our results with previous tidal dissipation number calculated in [2].

We start with the metric for static spherically symmetric background parametrized by two radial functions $v(r)$ and $\lambda(r)$:

$$g_{\mu\nu}^0 = \begin{pmatrix} -e^{v(r)} & 0 & 0 & 0 \\ 0 & e^{\lambda(r)} & 0 & 0 \\ 0 & 0 & r^2 & 0 \\ 0 & 0 & 0 & r^2 \sin^2(\theta) \end{pmatrix} \quad (4.1)$$

where we can relate $\lambda(r)$ to a mass function $m(r)$ inside the CO by $\lambda(r) = \frac{1}{1 - \frac{2m(r)}{r}}$. As we would like to remain general for now, we consider the stress energy tensor (SET) is given by two non-interacting viscous Landau fluids,

$$T_{\mu\nu} = \sum_{i=1}^2 T_{i\mu\nu} \quad (4.2)$$

where, the individual SETs are given by,

$$T_{i\mu\nu} = (\rho_i + p_i)u_{i\mu}u_{i\nu} + p_i g_{\mu\nu} - 2\eta_i P_{i\mu}^\alpha P_{i\nu}^\beta \sigma_{i\alpha\beta} - \zeta_i \nabla_\alpha u_i^\alpha P_{i\mu\nu} \quad (4.3)$$

Where η_i and ζ_i are the shear and bulk viscosity of the i th fluid. Furthermore we have defined

$$P_{i\mu\nu} = g_{\mu\nu} + u_{i\mu}u_{i\nu}$$

$$\sigma_{i\mu\nu} = \frac{1}{2} \left(\nabla_\mu u_{i\nu} + \nabla_\nu u_{i\mu} - \frac{2}{3} g_{\mu\nu} \nabla_\alpha u^\alpha \right)$$

For later convenience, we also define $p_{tot} = p_1 + p_2$ and $\rho_{tot} = \rho_1 + \rho_2$.

Now, we turn our attention to the zeroth order Einstein's equation for a static CO in equilibrium. We see the viscosity terms vanish in the static limit, and given equations of state $\rho_i = \rho_i(p_i)$, we can use the Tolman-Oppenheimer-Volkoff (TOV) equations [79] to solve for the background metric:

$$\frac{dm}{dr} = 4\pi\rho_{tot}r^2 \quad (4.4)$$

$$\frac{dp_i}{dr} = -\frac{(\rho_i + p_i)(m + 4\pi r^3 p_{tot})}{r(r - 2m)} = -\frac{(\rho_i + p_i)}{2} \frac{d\nu}{dr}, \quad (4.5)$$

with $p_i(\epsilon) = p_{i_c} - \frac{2\pi}{3}(3p_{tot} + \rho_{tot})\epsilon^2$, $m(\epsilon) = \frac{4\pi\epsilon^3\rho_0}{3}$ as initial conditions. Here $\rho_0 = \rho_{tot}(0)$, p_{i_c} is the central pressure, and ϵ is an arbitrarily small number. We can now solve these equations to determine the background metric $g_{\mu\nu}^0$. For this we integrate outward until we reach a cutoff pressure representing the surface of the star, roughly on the order of $10^{29} \frac{N}{m^2}$. The background metric components can then be determined using the definition of $m(r)$,

$$\frac{d\lambda}{dr} = \frac{\kappa r^2 \rho_{tot} e^\lambda - e^\lambda + 1}{r}, \quad \frac{d\nu}{dr} = \frac{e^\lambda + 8\pi r^2 p_{tot}}{r} \quad (4.6)$$

We will subsequently solve this system numerically for various choices of baryonic EoS and DM model.

We now consider a metric perturbation $g_{\mu\nu} = g_{\mu\nu}^0 + h_{\mu\nu}$ arising from the interior fluid's motion due to tidal forces. This perturbation assumes spherical symmetry of the background, and thus we can decompose $h_{\mu\nu}$ in the irreducible representation of the SO(3) group, i.e. scalar, vector and tensor spherical harmonics built from $Y_{lm}(\theta, \phi)$. Furthermore, we can distinguish even and odd parity terms. We are specifically interested in tidal deformations, which are even parity terms that at lowest order in the multi-pole expansion appear at $l = 2$. We can choose $m = 0$ due to axial symmetry of the background. Working in the Regge-Wheeler gauge, the perturbation can be parameterized as

$$h_{\mu\nu} = -\left(\frac{r}{R}\right)^2 Y_2(\theta) e^{-i\omega t} \begin{pmatrix} H_0(r)e^{v(r)} & -i\omega H_1(r) & 0 & 0 \\ -i\omega H_1(r) & H_2(r)e^{\lambda(r)} & 0 & 0 \\ 0 & 0 & r^2 K(r) & 0 \\ 0 & 0 & 0 & r^2 K(r) \sin^2 \theta \end{pmatrix} \quad (4.7)$$

where R is the radius of the star, and we have only considered the dominant $l = 2$ mode.

We can now substitute the perturbed metric into the Einstein field equations to obtain, at leading order in perturbation, $\delta G_{\mu\nu} = \delta(R_{\mu\nu} - \frac{1}{2}Rg_{\mu\nu}) = \kappa\delta T_{\mu\nu}$, where, the variation of the

Einstein tensor $\delta G_{\mu\nu}$ is given by,

$$\begin{aligned} \delta G_{\alpha\beta} = & \frac{1}{2} \left(g_{\alpha\beta} h^{\gamma\delta} R_{\gamma\delta} - h_{\alpha\beta} R - h^{\gamma}_{\gamma;\alpha;\beta} + h_{\beta}^{\gamma}_{;\alpha;\gamma} + h_{\alpha}^{\gamma}_{;\beta;\gamma} \right. \\ & \left. - h_{\alpha\beta}{}^{;\gamma}{}_{;\gamma} + \frac{1}{2} g_{\alpha\beta} g^{\gamma\delta} h^{\epsilon}_{\epsilon;\gamma;\delta} - g_{\alpha\beta} g^{\gamma\delta} h_{\gamma}{}^{\epsilon}_{;\delta;\epsilon} + \frac{1}{2} g_{\alpha\beta} g^{\gamma\delta} h_{\gamma\delta}{}^{;\epsilon}{}_{;\epsilon} \right) \end{aligned} \quad (4.8)$$

where, $R_{\mu\nu}$ and R are Ricci tensor and Ricci scalar respectively, and $;$ denote covariant derivative ∇_{μ} defined with respect to background metric $g_{\mu\nu}^0$.

To solve the first order in perturbation equation we need to obtain the perturbed stress energy tensor $\delta T_{\mu\nu}$ which in turn requires the perturbations in velocity δu^{μ} , density $\delta\rho$ and pressure δp . We start by considering that the unperturbed fluid's 4-velocity has no spatial component and from normalization it simply reads,

$$u^{\mu} = \left(e^{-\frac{1}{2}v(r)}, 0, 0, 0 \right) \quad (4.9)$$

We now consider the perturbation of this 4-velocity. To this end we define the fluid displacement vector ξ^{μ} arising due to the external tidal field as [80, 81]

$$\xi^{\mu} \equiv (\xi^t, \xi^r, \xi^{\theta}, \xi^{\phi}) = e^{-i\omega t} \left(\frac{r}{R} \right)^2 \left(0, \frac{e^{-\lambda/2} W}{r} Y_2(\theta), -\frac{V}{r^2} Y_2'(\theta), 0 \right) \quad (4.10)$$

where, the functions $W(r)$ and $V(r)$ describes the radial displacement. There is no azimuthal displacement or axisymmetric tides ($m = 0$) due to the non-rotation of the NS, and here we have decomposed the functions in terms of spherical harmonics. We can now calculate the fluid perturbation using $\delta u^{\mu} = u^{\nu} \nabla_{\nu} \xi^{\mu}$ to obtain:

$$\delta u^{\mu} = - \left(\frac{r}{R} \right)^2 e^{-i\omega t} e^{-v/2} \left(\frac{1}{2} H_0 Y_2(\theta), \frac{i\omega}{r} e^{-\lambda(r)/2} W Y_2(\theta), \frac{i\omega}{r^2} V Y_2'(\theta), 0 \right) \quad (4.11)$$

To get to the density ($\delta\rho$) and pressure (δp) perturbations in the Eulerian frame, we first consider the co-moving frame. As the timescale for heating due to viscosity far exceeds the orbital timescale, the density perturbation of the fluid can be written down considering only reversible thermodynamic processes [82, 83],

$$\Delta\rho = -(p + \rho) \frac{\Delta\Omega}{\Omega}, \quad (4.12)$$

where Ω is the volume of a fluid element and defined as [2, 81],

$$\Delta\Omega/\Omega = \nabla_{\mu}^s \xi^{\mu} + \frac{\delta(g^s)}{2g^s} = -Y_2(\theta) \frac{e^{-i\omega t}}{2r^2} \left(H_2 + 2K - \frac{12V}{r^2} - \frac{2e^{-\lambda/2}[3W + rW']}{r^2} \right) \quad (4.13)$$

with g^s is the determinant of the induced metric on the spatial hypersurface, and ∇^s is the covariant derivative in terms of this induced spatial metric. For our diagonal background metric, to first order in perturbation, the induced metric is simply the 3×3 spatial part of $g_{\mu\nu}$. Changing

the co-ordinates to Eulerian coordinate system, we obtain,

$$\delta\rho = \Delta\rho - \xi^r \frac{d\rho}{dr} \quad (4.14)$$

Next, we look into the pressure perturbation. We start with defining adiabatic parameter γ relating the fractional variation of baryon number density to that of pressure as,

$$\frac{\Delta p}{p} = \gamma \frac{\Delta n}{n} = -\gamma \frac{\Delta v}{v}. \quad (4.15)$$

With this definition, we can write the the Eulerian variation in pressure as,

$$\delta p = -\gamma \frac{\Delta v}{v} p - \xi^r \frac{dp}{dr} \quad (4.16)$$

We will also need the perturbation of energy momentum conservation equation to solve for all the equations of motions. Again to linear order in the perturbations, we have

$$\delta(\nabla_\mu T_\nu^\mu) = -h^{\alpha\mu} T_{\alpha\nu;\mu} + g^{\alpha\mu} (T_{\alpha\nu;\mu} - \delta\Gamma_{\alpha\mu}^\beta T_{\beta\nu} - \delta\Gamma_{\nu\mu}^\beta T_{\alpha\beta}) = 0 \quad (4.17)$$

Combining all the results in the first order Einstein's equation $\delta G_{\mu\nu} = 8\pi\delta T_{\mu\nu}$ allows us to eliminate H_2 and H_1 defined in eqn. (4.7) in terms of other variables.

$$H_2 = H_0 - 32\pi i\omega e^{-\frac{\nu}{2}} (V_1\eta_1 + V_2\eta_2) \quad (4.18)$$

and

$$H_1(r) = \frac{-r}{6} \left(2H_0 - 2rK' + K \left(\kappa r^2 p_{tot} e^\lambda + e^\lambda - 7 \right) - 2\kappa \sum_{j=1}^2 \left(e^{\frac{\lambda}{2}} W_j (p_j + \rho_j) + 4i\omega e^{-\frac{\nu}{2}} V_j \eta_j \right) \right) \quad (4.19)$$

After simplifications, the system of equations reduces to

$$H_0' + \frac{H_0 (8\pi r^2 p_{tot} e^\lambda + e^\lambda + 1)}{r} - K' - \frac{2K}{r} - \frac{2\kappa i\omega e^{-\frac{\nu}{2}} \sum_{j=1}^2 \eta_j \left((\kappa r^2 p_{tot} e^\lambda + e^\lambda + 1) V_j + r V_j' - e^{\frac{\lambda}{2}} W_j \right)}{r} + \omega^2 H_1 e^{-\nu(r)} = 0 \quad (4.20)$$

and

$$\begin{aligned}
& H_0' + \frac{H_0 e^\lambda (\kappa r^2 p_{tot} - \kappa r^2 \rho_{tot} + 8)}{2r} + K \left(\frac{\kappa r^2 p_{tot} e^\lambda - e^\lambda - 3}{r} \right) + \frac{K'}{2} (\kappa r^2 p_{tot} e^\lambda + e^\lambda - 3) \\
& - i\kappa\omega \sum_{j=1}^2 \left\{ \frac{\eta_j e^{-\frac{\nu}{2}}}{2r} \left[8(4e^\lambda + 1)V_j + V_j' (\kappa r^3 e^\lambda \rho_{tot} - r e^\lambda + r) - 2r^2 V_j'' + 4e^{\frac{\lambda}{2}} W_j + r^2 e^\lambda (H_0 - 4K) \right] \right. \\
& \quad \left. + r\eta_j e^{\lambda-\nu/2} \left[\frac{H_0}{2} + K - \frac{6V_j}{r^2} - \frac{e^{-\lambda/2}}{r^2} (3W_j + rW_j') \right] + e^{-\frac{\nu}{2}} \eta_j' \left(e^{\frac{\lambda}{2}} W_j - rV_j' \right) \right\} \\
& = -r\omega^2 e^{\lambda-\nu} \left(K - \kappa \sum_{j=1}^2 V_j (\rho_j + p_j) + \text{visc.} \right) \tag{4.21}
\end{aligned}$$

Eqs. (4.20) and (4.21) together forms a system of master equations for two independent perturbation quantities H_0 and K . Although, H_1 appears explicitly in these equations, one can see it can be eliminated using (4.19). Here *visc.* represents terms that contain shear viscosity, η_j and the subscripts 1, 2 label the two fluids.

Since our aim is to match the full theory result to the EFT order by order in ω to obtain tidal love numbers up to NNLO, we expand the metric perturbations in powers of ω , keeping terms up to second order in frequency.

$$H_0(r) = H^{(0)}(r) + \omega H^{(1)}(r) + \omega^2 H^{(2)}(r) + O(\omega^3) \tag{4.22}$$

and

$$K(r) = K^{(0)}(r) + \omega K^{(1)}(r) + \omega^2 K^{(2)}(r) + O(\omega^3) \tag{4.23}$$

Substituting back the expansions in the master equation, lets us obtain the differential equations order by order in ω .

4.1 Solution at $O(\omega^0)$

At LO (i.e. $O(\omega^0)$) the master equations read:

$$H^{(0)'} + \frac{H^{(0)} (8\pi r^2 p_{tot} e^\lambda + e^\lambda + 1)}{r} - K^{(0)'} - \frac{2K^{(0)}}{r} = 0 \tag{4.24}$$

and

$$H^{(0)'} + \frac{H^{(0)} e^\lambda (\kappa r^2 p_{tot} - \kappa r^2 \rho_{tot} + 8)}{2r} + K^{(0)} \left(\frac{\kappa r^2 p_{tot} e^\lambda - e^\lambda - 3}{r} \right) + \frac{K^{(0)'}}{2} (\kappa r^2 p_{tot} e^\lambda + e^\lambda - 3) = 0 \tag{4.25}$$

These equations match with [25] up to some differences in convention. To solve the LO master equations, one needs to specify boundary conditions *near* the center ($r \rightarrow 0$) of the star to avoid

the pole at the center. To this end, we solve the master equations via power series expansion near the origin. We insert Taylor series expansions for all functions appearing in the master equations and solve for the power series expansions of H_0 and K around $r = 0$.

$$\begin{aligned}
H^{(0)}(r) = 1 - \frac{-4\pi(99p^2 + 36p\rho + \rho^2) + 9\rho''}{42(3p + \rho)}r^2 \\
+ \frac{1}{7560(3p + \rho)^2} \left[160\pi^2(3p + \rho)^2(414p^2 + 57p\rho + 43\rho^2) \right. \\
\left. - 24\pi(201p - 28\rho)(3p + \rho)\rho'' - 54(\rho'')^2 + 105(3p + \rho)\rho^{(4)} \right] r^4 + \mathcal{O}(r^6)
\end{aligned} \tag{4.26}$$

$$\begin{aligned}
K^{(0)}(r) = 1 + \frac{8\pi(-6p^2 + p\rho + \rho^2) + 3\rho''}{14(3p + \rho)}r^2 + \frac{1}{7560(3p + \rho)^2} \left[800\pi^2(3p + \rho)^2(18p^2 - 3p\rho + 11\rho^2) \right. \\
\left. + 120\pi(3p + \rho)(3p + 20\rho)\rho'' - 54(\rho'')^2 + 105(3p + \rho)\rho^{(4)} \right] r^4 + \mathcal{O}(r^6)
\end{aligned} \tag{4.27}$$

Here the pressure, densities, and their derivatives are all evaluated at the origin and we have dropped the $_{tot}$ subscripts for conciseness. The sixth order terms are too large to be given here and are provided in a supplemental Mathematica notebook. The only constraint on the arbitrary constant term is that $H^{(1)}(0) = K^{(1)}(0)$, thus we choose a value of unity which will not affect our final calculated observables. We show the convergence of the numerical and series solution near the origin for an illustrative case in Fig. 1.

We use these near center solutions for H_0 and K as boundary condition for the numerical integration for the full solution of the master equation, with the the other boundary condition being put at the surface of the star, $r = R_s$. The starting point near the center for numerical integration must be chosen to obtain an optimal agreement between the numerical and series solution and their derivatives near the origin. For most NS, starting the numerical integration 10-100 meters from the origin avoids numerical instability and matches smoothly onto the series expansion. In general, with increasing compactness the matching point moves closer to the origin.³

4.2 Solution at $O(\omega^1)$

Next, the $O(\omega^1)$ equations are obtained by taking $\omega^2 \rightarrow 0$ and substituting in the zeroth order solutions in the RHS source terms. We still need to find the static limit of the functions W and V which appear at this order in ω in our master Eqns. (4.20) and (4.21). Closely following [2], we use conservation equations $\nabla_\mu T_\theta^\mu = \nabla_\mu T_r^\mu = 0$ for each fluid and take the limit $\omega \rightarrow 0$ to

³In this case, the pole at the origin could be avoided all together by multiplying by r and making the Cauchy-Euler substitution $r \rightarrow e^s$. However, we find that the resulting numerical solution does not match the aforementioned series solution near the origin and has a divergent derivative as $r \rightarrow 0$. We invoke the regularity of the metric at the origin to disregard this method and instead we use the series solution to begin the numerical integration away from the origin.

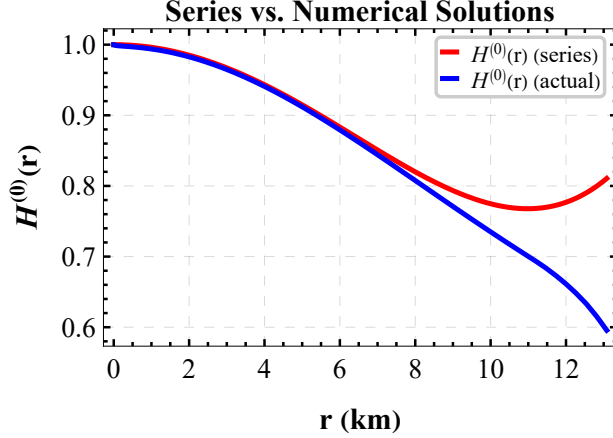


Figure 1: Plot of $H^{(0)}(r)$. Series expansion (blue) and full numerical solution (orange) for $2 M_{\odot}$ NS .

obtain alternative expressions for δp and $\delta \rho$. Equating these to our previous expressions for these quantities gives us,

$$\frac{\Delta v_j}{v_j} = 0, \quad W_j = \frac{r H^{(0)}(p_j + \rho_j) e^{\lambda/2}}{2p'_j} \text{ as } \omega \rightarrow 0 \quad (4.28)$$

which uses the assumption that internal reactions inside the star are very slow compared to ω even as we approach the static limit. In this case the adiabatic parameter γ is given as [2],

$$\gamma_j = c_{ins_j}^2 \frac{p_j + \rho_j}{p_j} \text{ with } c_{ins_j} = \frac{\partial p_j}{\partial \rho_j} \quad (4.29)$$

and the fraction of each particle type in the fluid is held constant in this slow reaction regime.

Note that by substitution of the T.O.V equation Eq. 4.5 for each fluid, in static limit we have $W_j = \frac{-r H^{(0)} e^{\lambda/2}}{\nu'}$ indicating the radial fluid perturbations for each fluid are identical. We can then use $\frac{\Delta v_j}{v_j} = 0$ to obtain the static limit of V_j in terms of W , H_0 , and K for both fluids. The expression for the static limit of V can be found in [2] and we see that the angular fluid perturbation V is also the same for each fluid.

Now having the source terms for the 1st order equations, we use the same technique as for the $O(\omega^0)$ result and find a Taylor expansion for $H^{(1)}$ and $K^{(1)}$ defined through Eq. 4.22 and Eq. 4.23 around $r = 0$ and begin the numerical integration at a point away from the origin. Following the same procedure for the 1st order equations, and additionally substituting in series expansions in r for W and V in the static limit, we find that for the constant term in the Taylor expansion, the only constraint is,

$$K^{(1)}(0) = H^{(1)}(0) + \frac{6e^{-\nu(0)/2}(\eta_1(0) + \eta_2(0))}{3p_{tot}(0) + \rho_{tot}(0)}. \quad (4.30)$$

It is easy to see, without loss of generality we can set $H^{(1)}(0) = 0$.

Continuing the expansion to quintic order, we find that only the quadratic and quartic terms in r are nonzero. Here we give the quadratic expansion assuming a non-viscous second fluid. The full general coefficients are given in the supplemental notebook. Again, we drop the $_{tot}$ subscript,

and all quantities are evaluated at the origin.

$$\begin{aligned}
H^{(1)}(r) = & \frac{e^{-\nu/2}}{175 \kappa (3p + \rho)^4} \left[\eta_1 \left(50 \kappa^2 (3p + \rho)^4 + 15 \kappa (3p + \rho) (6p + \rho) \rho'' - 351 (\rho'')^2 \right. \right. \\
& + 75 (3p + \rho) \rho^{(4)} \left. \left. + \frac{75}{2} (3p + \rho) \left([\kappa (3p + \rho) (7p + 5\rho) + 6 \rho''] \eta_1'' \right. \right. \right. \\
& \left. \left. \left. - 2(3p + \rho) \eta_1^{(4)} \right) \right] r^2 + O(r^4)
\end{aligned} \tag{4.31}$$

$$\begin{aligned}
K^{(1)}(r) = & \frac{6e^{-\nu/2} \eta_1}{3p + \rho} + \frac{e^{-\nu/2}}{350 \kappa (3p + \rho)^4} \left[\eta_1 \left(50 \kappa^2 (2p - 3\rho) (3p + \rho)^3 \right. \right. \\
& + 9 \left(5 \kappa (3p + \rho) (17p + 5\rho) - 78 \rho'' \right) \rho'' + 150 (3p + \rho) \rho^{(4)} \left. \left. \right. \right. \\
& \left. \left. \left. - 150 (3p + \rho) \left([\kappa (3p + \rho) (7p + \rho) - 3 \rho''] \eta_1'' + (3p + \rho) \eta_1^{(4)} \right) \right] r^2 + O(r^4)
\end{aligned} \tag{4.32}$$

These functions at arbitrary r can be solved numerically using the boundary conditions in the same manner as the LO result.

4.3 Solution at $O(\omega^2)$

The second order equations are only valid for the non-viscous case, $\eta_j \rightarrow 0$, as mentioned previously. Therefore, we take all viscous terms (which includes all ω^1 terms) to zero when solving for $H^{(2)}$ and $K^{(2)}$. Similar to the LO and NLO order calculation, we substitute the static limit perturbations in the ω^2 source terms and solve for the second order metric perturbations, utilizing a Taylor series expansion of the solution near the origin to begin the numerical integration.

At this order, we obtain $H^{(2)}(0) = K^{(2)}(0)$ and again choose unity as the constant term without loss of generality. Similarly, proceeding up to quintic order, only the quadratic and quartic terms in r are nonzero, the latter which are provided in the supplemental notebook.

$$\begin{aligned}
H^{(2)}(r) = & 1 + \frac{1}{420} \left[-5 \kappa (33p + \rho) \right. \\
& \left. + \frac{54 e^{-\nu} (13p + 3\rho) \rho''}{\kappa (3p + \rho)^3} + \frac{5 e^{-\nu} (-39p + 5\rho + 18 e^\nu \rho'')}{3p + \rho} \right] r^2 + O(r^4)
\end{aligned} \tag{4.33}$$

$$\begin{aligned}
K^{(2)}(r) = & 1 + \frac{1}{210} \left[15 \kappa (-2p + \rho) \right. \\
& \left. + \frac{27 e^{-\nu} (13p + 3\rho) \rho''}{\kappa (3p + \rho)^3} - \frac{5 e^{-\nu} (9p + \rho - 9 e^\nu \rho'')}{3p + \rho} \right] r^2 + O(r^4)
\end{aligned} \tag{4.34}$$

To obtain specific numerical solutions, we need to supply equations of state for the fluids. We can then integrate the background T.O.V. equation and solve for the background metric, and the pressure and density profiles for the fluids. Then, with the series expansions for the perturbed metric at the center, we can solve for the metric for the entire interior of the star up to 2nd order in ω . In the next section we describe the observable we compute using the interior solution which will enable us to extract the TLNs. In section 5, we present explicit numerical results.

4.4 Surface reflectivity and compactness

Having obtained the background metric and metric perturbations in the interior, we need to match this solution, or any appropriate function of this solution to the solution in the exterior. As explained in section 3, this is done by computing the coefficients of the small frequency expansion of the matching parameter T , along with the compactness, which we then use in the BHPT scattering amplitude result eqns. (3.9) and (3.10).

Here we relate the interior solutions obtained in the previous section, namely the background metric and the metric perturbations to the compactness and the parameter T . The compactness $\mathcal{C} = M/R_s$ can be computed directly from the background metric solution. For computing T , we start by writing the RW variable $X(r)$ introduced in eqn. (3.1) which can be written inside the star (and at the surface) in terms of the metric perturbation functions H_0 and K defined in the previous section [84],

$$X = \frac{-1}{(n+1)M} \left[\{-n(n+1)r(r-3M)\}K + (n+1)r(nr+3M)e^{-\lambda}H_0 \right] \quad (4.35)$$

and its derivative

$$X' = \frac{1}{-(n+1)M} \left[n(n+1)\{(n+1)r-3M\}K + \{-n(n+1)^2r-3(n+1)Me^{-\lambda}\}H_0 \right] \quad (4.36)$$

where $n = (l-1)(l+2)/2 = 2$ for $l = 2$. We now expand X and its derivative in ω ,

$$X^{(n)} = X_0^{(n)} + i\omega R X_{\omega^1}^{(n)} + (\omega R)^2 X_{\omega^2}^{(n)} + \dots$$

where, $n = 0$ denotes X and $n = i$ denotes the i^{th} derivative of RW variable w.r.t. r . Substituting the expansion of RW variable in the definition of the matching parameter T given in eqn. (3.5),

$$\begin{aligned} T &= \left. \frac{r}{X} \frac{dX}{dr_*} \right|_{r=R_S} = \left. \frac{re^{-\lambda}}{X} \frac{dX}{dr} \right|_{r=R_S} \quad (4.37) \\ &= re^{-\lambda} \left[\frac{X'_0}{X_0} + \frac{-X_1X'_0 + X_0X'_1}{X_0^2} \omega + \left(\frac{-X_1X'_1}{X_0^2} + \frac{X'_0(X_1^2 - X_0X_2)}{X_0^3} + \frac{X'_2}{X_0} \right) \omega^2 + \dots \right] \\ &\equiv T_0 - (iR\omega)T_1 - (R\omega)^2T_2 + \dots \end{aligned}$$

We can then calculate the coefficients in the expansion of T for a specific EoS for NS and NS+DM systems. This will allow us to calculate ‘reflectivity’ of the stellar surface using eqn. (3.6).

5 Dynamical Tidal response from EFT matching

In the previous sections, we have derived the master equations for stellar perturbations and have seen how they relate to the surface reflectivity. This surface reflectivity, with the BHPT scattering amplitude expression, can then be matched with the EFT result to obtain the static and dynamic TLNs. This is achieved by matching the scattering amplitude obtained from EFT (with 2-PM corrections), eqn. (2.26) and the corresponding result from BHPT eqns. (3.8)-(3.10), written in terms of the compactness \mathcal{C} and reflectivity parameter T . We will now focus on numerically solving NS and NS+DM systems with various equations of state for nuclear matter and DM. We then use the results obtained in the previous sections to obtain tidal love numbers for these choices. We will present specific results in the form of rescaled tidal love numbers, given by

$$k_2^e = \frac{3\mathcal{C}^5}{2}\Lambda_{\omega^0}^E \quad \nu_2^e = \frac{3\mathcal{C}^6}{2}\Lambda_{\omega^1}^E \quad \kappa_2^e = \frac{3\mathcal{C}^7}{2}\Lambda_{\omega^2}^E \quad (5.1)$$

These rescaled TLNs separate the contributions from compactness and internal structure on the total tidal deformability.

5.1 Neutron stars admixed with fermionic dark matter

In the case of an NS, the exact description of interior nuclear matter remains unknown; however, various proposed baryonic EoS have been theorized and have been tabulated in the CompOSE database [85]. To facilitate the numerical solving process, we fit a piecewise polytropic EOS ($\rho = Kp^\Gamma$) to these EOS. We find that at low pressures, a simple polytrope easily fits the data. At greater pressure and density, it is necessary to fit a sum of polytropes $\rho = K_1 p^{\Gamma_1} + K_2 p^{\Gamma_2}$ to obtain an accurate fit of the data. All the equations of state we consider are for low temperature stars, $10^5 - 10^7$ Kelvin. This is appropriate as the vast majority of merging neutron stars are mature enough to have cooled down to this temperature range.

For baryonic matter, the shear viscosity predominantly arises from electron-electron scattering [86] and is approximated by the fitting formula [87]

$$\eta = 270 \frac{\rho^2}{T^2} \quad (\text{m}^{-1}) \quad (5.2)$$

where T is the temperature of the NS. Specifically, we will take $T = 10^5$ K in the following viscosity calculations.

Next we consider the dark matter EoS. We start our discussions with fermionic DM [88, 89] which corresponds to the traditional cold DM (CDM) paradigm. We model the dark matter EOS as a single polytrope, and will only consider non-viscous dark matter for simplicity. We will treat the fermionic DM as a non-relativistic Fermi gas, valid for large particle masses. A simple assumption is to use a DM EOS analogous to that of normal matter in a white dwarf star. This is given by the following parametric equations [90, 91],

$$\rho = K_{DM}[\sinh(t) - t] \quad (5.3)$$

$$p = \frac{K_{DM}}{3}[\sinh(t) - 8 \sinh(\frac{t}{2}) + 3t] \quad (5.4)$$

where K_{DM} is given by:

$$K_{DM} = \left(\frac{M_{DM}^4}{32\pi^2 \hbar^3} \right)$$

and M_{DM} is the mass of the DM particle. For the range of densities and pressures in a NS, one can rewrite these equations as a polytropic EoS in $G = c = 1$ units:

$$\rho = 0.00752 \left(\frac{M_{DM}}{1\text{GeV}} \right)^{\frac{4}{3}} p^{\frac{2}{3}} \quad (5.5)$$

This polytrope is applicable throughout the stars we will consider. However, if the core is very dense and the Fermi energy exceeds M_{DM} , then in this ultra-relativistic limit we obtain a different polytrope which isn't relevant for our purposes.

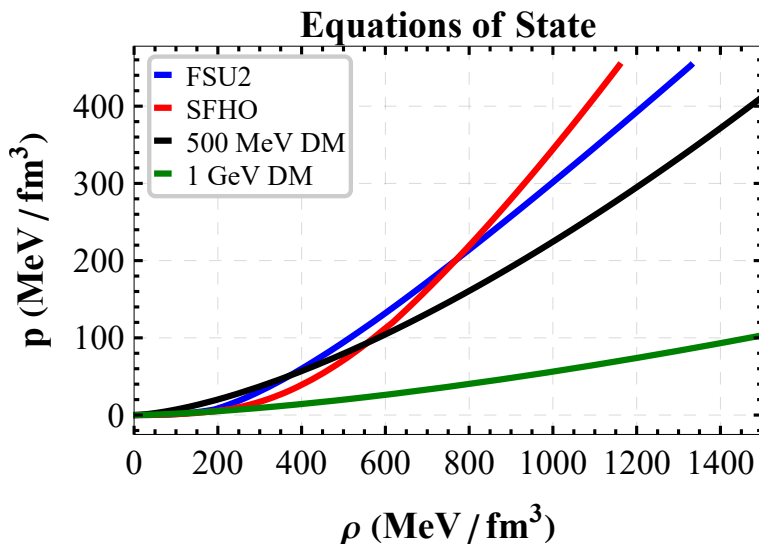


Figure 2: Representative EoS for NS baryonic matter and fermionic DM as a function of energy density. Blue and red curves represent FSU2 and SFHO baryonic EoS while the black and green curves represent EoS for Fermionic DM fluids with particle masses of 500 MeV and 1 GeV respectively.

In Fig. 2 we have plotted some representative EoS of baryonic nuclear matter - FSU2 and SFHO as well as the EoS of fermionic DM for two different masses - 500 MeV and 1 GeV. We focus on fermionic DM particles of mass $\sim O(\text{GeV})$ as this is found to give the richest parameter space consistent with observation. This mass range can be motivated by an attempt to explain matter-antimatter asymmetry by considering a baryon-like dark sector with a corresponding asymmetry

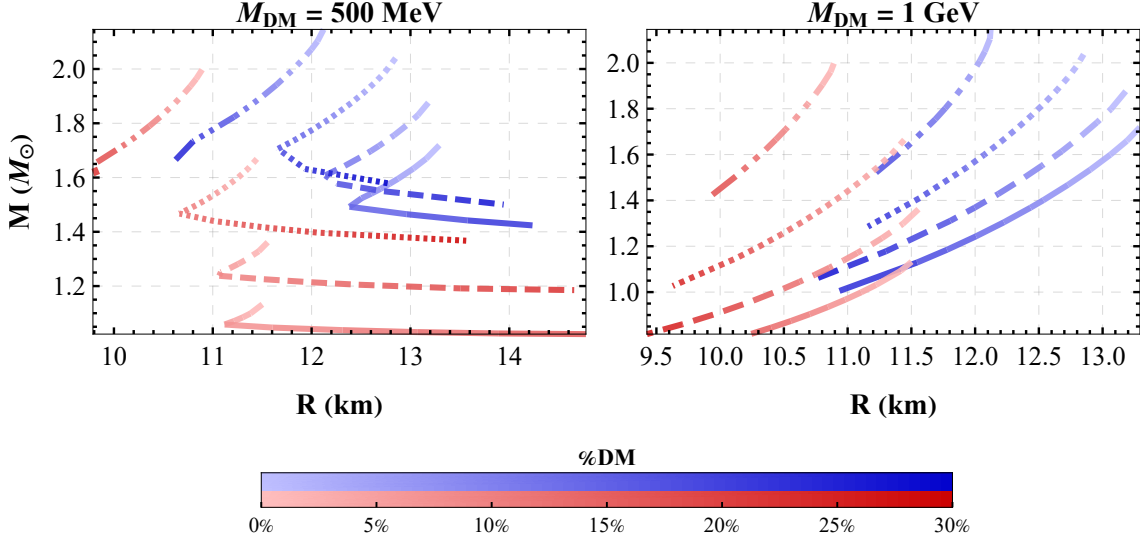


Figure 3: Mass-radius relationship for fermionic DM admixed neutron star. Two baryonic EoS, FSU2 and SFHO, are denoted with blue and red curves respectively. Each line progresses from light to darker shades, representing lower DM mass fraction (%DM) and higher DM mass fractions respectively. Solid, dashed, dot-dashed, and dotted lines represent central baryonic densities of 425, 500, 600, and $1000 \frac{\text{MeV}}{\text{fm}^3}$ respectively.

[92].

With these EoS, we can solve the background TOV equations to find mass-radius relationships for a family of NS with various central densities and dark matter fractions. Qualitatively, while the DM gravitationally behaves the same as normal matter, its pressure no longer supports the NS against baryonic matter contraction and vice versa. This effective softening of the star implies that the maximum supported mass for an admixed NS will be lower than that of a pure NS [90].

This can be seen in Fig. 3, where we have plotted the mass-radius relation for two different values of admixed fermionic DM mass, $M_{\text{DM}} = 500\text{MeV}$ and 1GeV with varying mass fraction of DM (%DM) of total stellar mass denoted by gradual darkening for each colored curve. For each curve the lightest end denotes the result for pure NS (i.e 0% DM mass). The blue and red curves represent FSU2 and SFHO EoS respectively, while the each line style denote a particular central baryon density for given EoS. From the plot, we can see that with increasing DM particle mass(M_{DM}) and DM mass fraction, the allowable total mass of the DM admixed NS drops significantly as previously shown in literature [93]. The range of radii however is less affected, leading to a significant decrease in compactness.

Next, we determine how the TLNs are affected by the various NS+DM parameters. This requires numerically integrating the perturbative master equations for different DM particle masses and mass fractions to determine how the boundary conditions at the surface of the NS change. These equations mathematically have the same form as in the case of pure normal matter- the introduction of non-viscous DM simply modifies these equations by changing the total pressure and density, p_{tot} and ρ_{tot} .

In Fig. 4, we have plotted the static and dynamical TLNs along with TDNs as a function

ρ_0	%DM	M	R (km)	R_{DM} (km)	C	k_2^e	$\nu_2^e (\times 10^3)$	κ_2^e
425	0	1.72	13.29	0	0.19	0.087	0.032	0.16
425	1.47	1.67	13.16	8.94	0.19	0.088	0.033	0.17
425	5.82	1.58	12.79	10.98	0.18	0.086	0.032	0.18
425	12.11	1.49	12.3	12.38	0.18	0.082	0.03	0.2
425	21.36	1.42	11.68	14.23	0.15	0.032	0.009	0.29
650	0	2.04	12.85	0	0.24	0.052	0.00002	0.13
650	1.61	1.99	12.74	7.95	0.23	0.053	0.021	0.14
650	5.14	1.9	12.47	9.44	0.22	0.053	0.021	0.15
650	11.1	1.78	12.01	10.57	0.22	0.052	0.02	0.16
650	22.27	1.63	11.19	11.93	0.2	0.037	0.013	0.19
1000	0	2.15	12.12	0	0.26	0.034	0.015	0.12
1000	1.43	2.1	12.06	6.8	0.26	0.035	0.015	0.12
1000	4.55	2.02	11.87	8.08	0.25	0.035	0.015	0.13
1000	9.78	1.9	11.51	9.05	0.24	0.035	0.015	0.14
1000	19.7	1.73	10.8	10.08	0.24	0.034	0.015	0.15

Table 1: Tabulated numerical values of observables for a 500 MeV fermionic DM mixed with NS with FSU2 equation of state. We consider three distinct values for the central density ρ_0 in units of $\frac{\text{MeV}}{\text{fm}^3}$ with increasing mass fraction of DM in each case.

of compactness of the admixed star. As before, we have considered two different EoS for the NS baryonic matter, with blue and red curves representing FSU2 and SFHO EoS respectively, with the various line styles representing different central densities. We have considered two different DM mass of 500MeV and 1 GeV. We have also considered the effect of percentage of total DM mass of total stellar mass, denoted by %DM and indicated by the lighter to darker shading of the curves, with the lightest shade indicating 0% DM contribution i.e pure NS results. Further, we have tabulated the numerical results in Table 1.

From Fig. 4, we can see that static TLN (k_2^e) decreases with increasing DM concentration. This can be explained by a dense core forming at the center of the NS as DM increases, which shifts the mass distribution toward the center of the star. This reduces the amount of mass exposed to the stronger tidal field near the surface, accounting for the lowered tidal deformability. The similar decrease in ν_2^e with increasing percentage of DM is due to the dark matter core increasing the baryon density there and increasing the rigidity of the NS due to gravitational attraction. This decreases the magnitude of fluid displacement within the NS and thus the dissipative energy loss. Interestingly, the rescaled dynamical TLN instead increases with increasing DM admixture. To interpret this, we recall that κ_2^e is correlated with the magnitude of the delayed tidal response solely due to internal structure, after controlling for compactness. As dark matter concentration increases we can understand this increased tidal delay as due to the non-interaction of DM with baryonic matter, removing interactions that would otherwise work to more quickly synchronize a purely baryonic star with the external tidal field.

We also notice that increasing M_{DM} , which represents a softening of the DM EOS, results in an overall decrease in compactness as qualitatively expected. However, the effect on the static TLN and dissipation number with increasing DM percentage is less pronounced. This is likely due

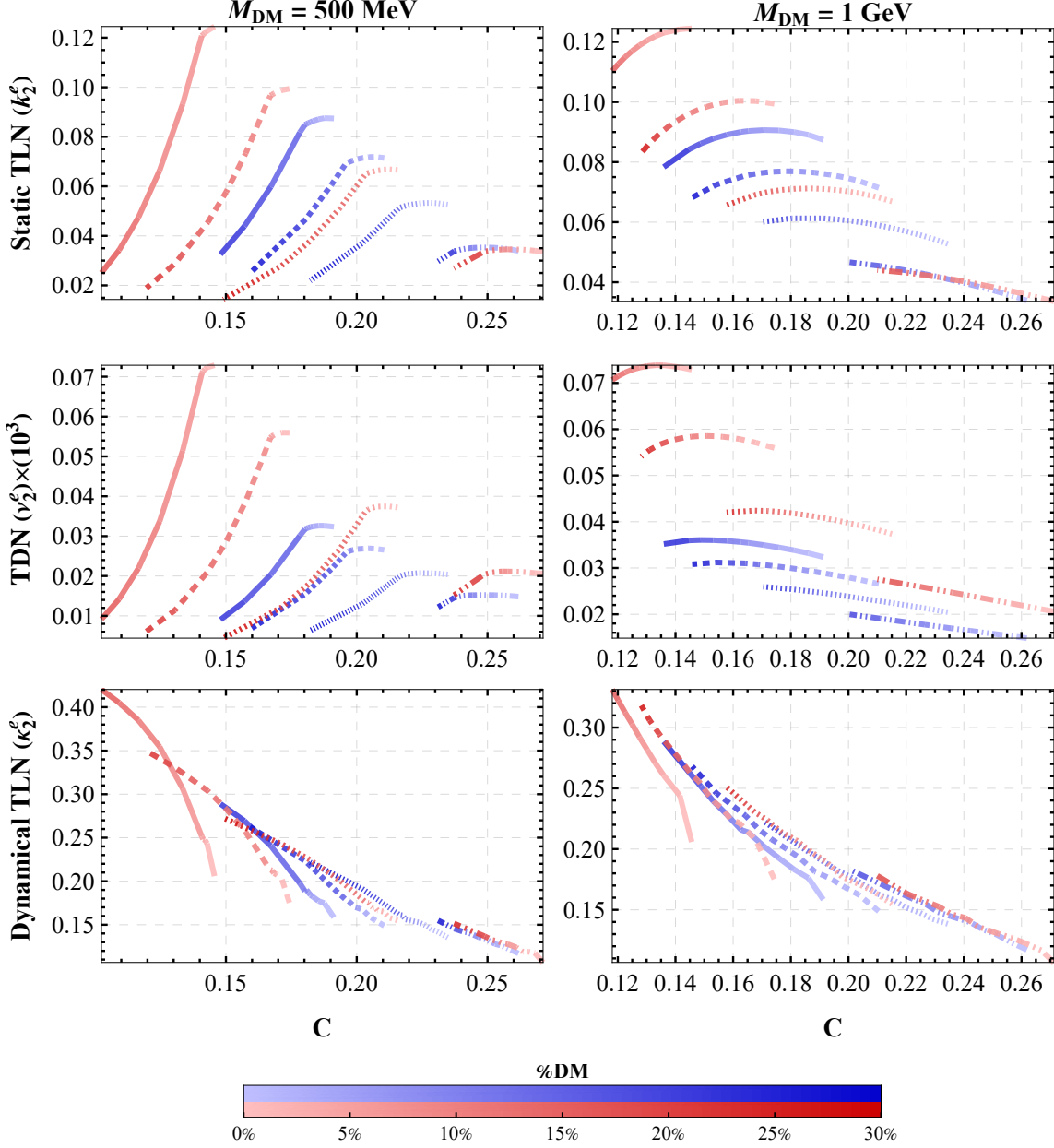


Figure 4: Tidal responses for fermionic DM admixed NS as a function of compactness for two different DM mass, $M_{\text{DM}} = 500\text{MeV}$ and 1GeV . We have considered FSU and SFHO EoS for baryonic matter, denoted by blue and red curves respectively. Solid, dashed, dot-dashed, and dotted lines represent different central baryonic densities of 425, 500, 600, and $1000 \frac{\text{MeV}}{\text{fm}^3}$ respectively. For each curve, color shade indicates the DM percentage of total stellar mass, with lighter shades representing lower percentages and darker shades denoting higher percentages.

to the compactness reaching such a degree, that adding more DM doesn't significantly overcome the effect of the increased baryonic pressure in order to bring baryonic matter closer to the center. Thus k_2^e and ν_2^e which are most sensitive to mass distribution within the NS roughly plateau in

this regime.

It is further noted that above a certain critical mass fraction ($\%DM_{\text{crit}}$), the dense DM core becomes so dominant that the radius of the star abruptly shrinks to $\sim 1\text{km}$ and below. We exclude these unobserved NS from the representative data tables. For fermion masses roughly below $\sim 300\text{MeV}$, the DM instead forms a diffuse halo around the star which drastically reduce the compactness of the NS. GW observations effectively rule out such halos created by even small percentages of fermionic dark matter [94].

5.2 Neutron Stars Admixed with Bosonic Dark Matter

While in the CDM paradigm, DM is modeled as a massive fermionic particle, observational discrepancies have resulted in alternative models like ultralight bosonic DM (see [95, 96] for a detailed discussion). In contrast to fermionic dark matter in the GeV range, ultralight bosonic dark matter tends to form diffuse halos around the NS. In our work, we consider the bosonic DM to be given by an ultralight scalar field with quartic self-interaction and given by the equation of state [97, 98],

$$p = \frac{2\pi l_{DM}}{m_{DM}^3} \rho^2 \equiv A_\chi \rho^2 \quad (5.6)$$

Where l_{DM} is the dark matter particle's scattering length and m_{DM} is its mass.

As before, we treat DM as a non-viscous fluid and numerically integrate the master equations. We will consider the range $0.4 < A_\chi < 100$ (in $\frac{\text{m}^5}{\text{kg s}^2}$) as this has been shown to produce identifiable effects in admixed NS [97]. In Fig. 5 we have plotted the mass-radius relations for the bosonic

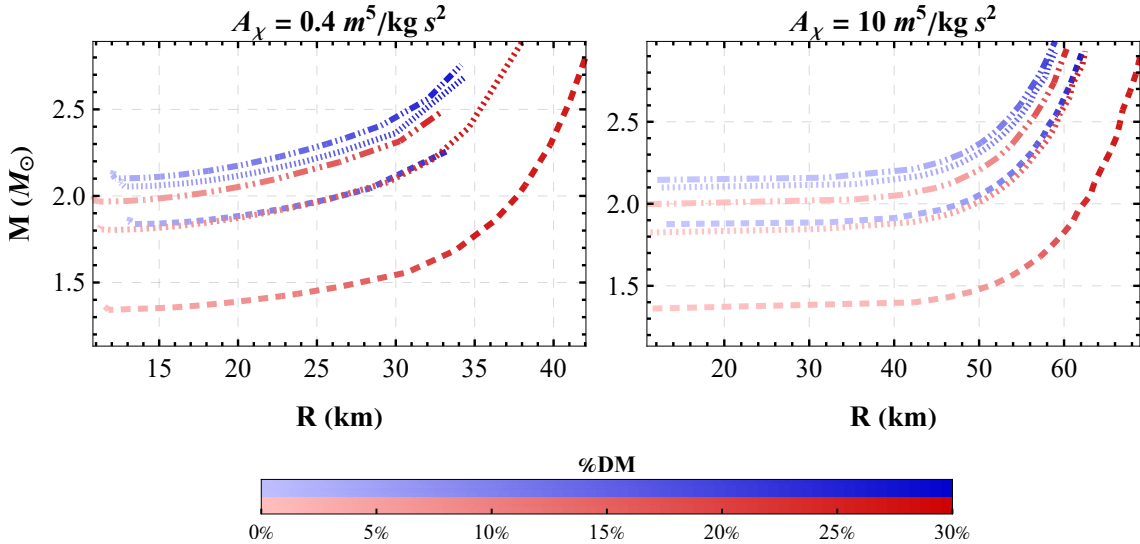


Figure 5: Mass-radius relationship for bosonic DM admixed neutron star. We consider two NS baryonic EoS — FSU2 and SFHO, given by blue and red respectively. Each curve progresses from lighter to darker shades, indicating a lower or higher DM percentage contribution to the total mass of the system. For each color solid, dashed, and dot-dashed lines represent central baryonic densities of 500, 750, and $1000 \frac{\text{MeV}}{\text{fm}^3}$ respectively.

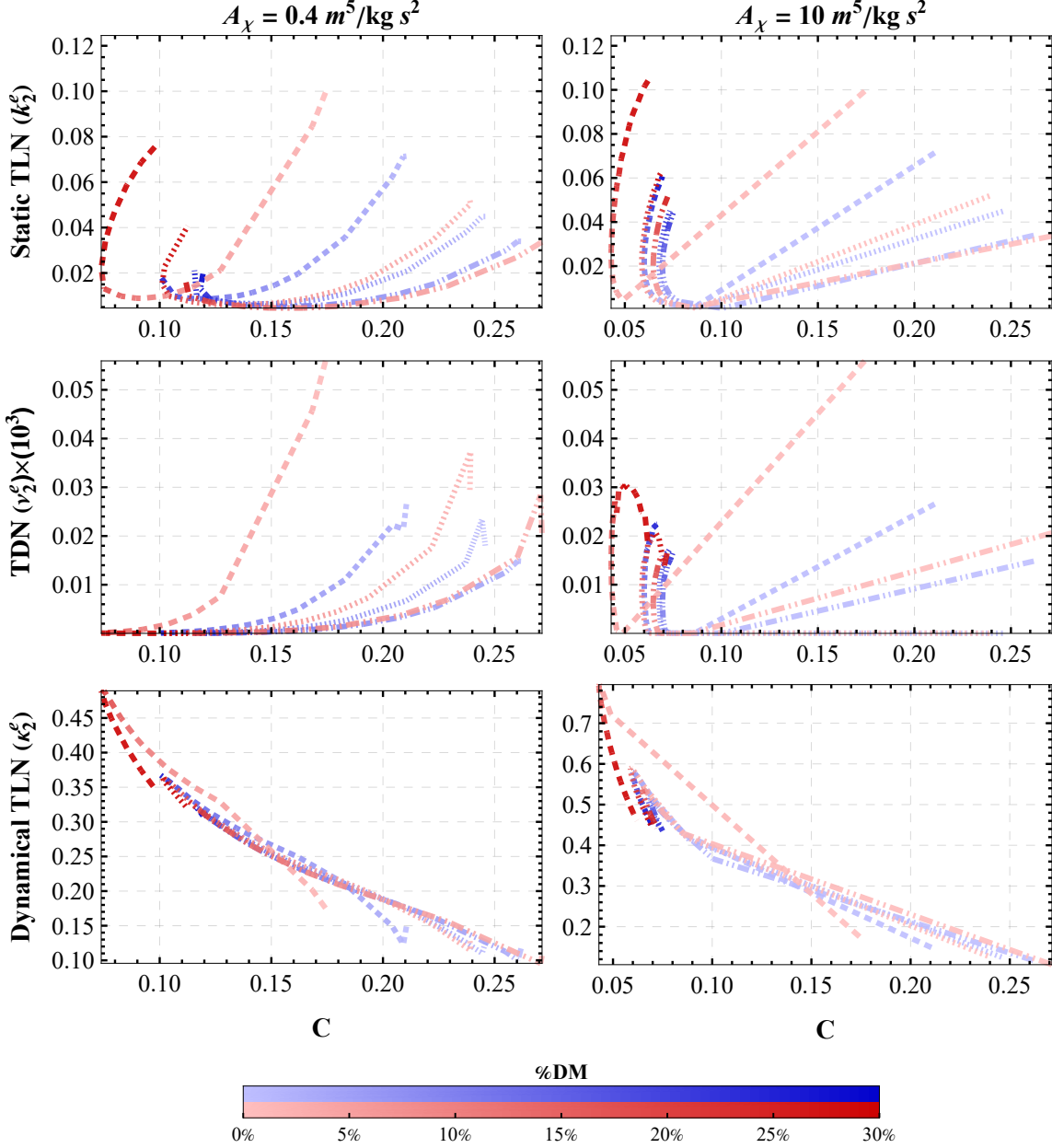


Figure 6: Tidal Love numbers for bosonic DM admixed neutron star. FSU and SFHO baryon EoS are blue and red respectively. Each curve progresses from lighter shades (representing lower DM percentage) to darker (higher %DM) shades. Solid, dashed, and dot-dashed lines represent central baryonic densities of 500, 750, and 1000 $\frac{\text{MeV}}{\text{fm}^3}$ respectively.

DM admixed NS for two different values of A_χ and two different baryonic EoS, FSU2 and SFHO. One can see that owing to its lighter nature, bosonic DM forms a diffuse halo around the NS as expected, compared to fermionic DM admixed NS. It can also be seen explicitly in Table 2, where we have tabulated some representative results.

Next we move on to the calculation of tidal Love and dissipation numbers. We follow the

same procedure outlined in the last subsection and produce the result of the tidal responses in Fig. 6. As before we consider two different values of A_χ and two different baryonic EoS, FSU2 and SFHO, given by blue and red curves respectively. Further in line with the fermionic DM admixed NS, we have chosen three different central baryonic densities given by different line styles. We can see from the plots and the tabulated results, formation of the larger, diffuse halo reduces its compactness and initially the rescaled static tidal love number k_2^e decreases as well. However, above a critical amount of DM, k_2^e suddenly begins to increase again, signifying an increasing tidal response from the internal structure of the star after controlling for compactness. Note that inverse compactness remains the dominant contribution to tidal deformability, and so the total tidal deformability($\Lambda_{\omega_0}^E$) still monotonically increases with $\%DM$. Similar behavior is noted for the rescaled dissipation number; however for small enough A_χ there is no such rebound as the halo grows. This is consistent with the fermion DM case. In the case of NS with bosonic DM though, the rescaled dynamical TLN instead increases with increasing DM admixture, before reversing only at relatively high dark matter concentrations. The initial increase is consistent with that observed for fermionic DM. The reversal at large DM fraction is likely related to the extended diffuse halo becoming dominant there. This halo is evidently less responsive to the changing tidal field.

6 Summary and Outlook

In this paper, we have used a worldline EFT(wEFT) approach to compute dynamical tidal love numbers for static neutron stars and neutron stars admixed with dark matter. The TLNs are defined as Wilson coefficients of higher dimensional gauge invariant operators in a point particle wEFT. Modeling stars as non-viscous fluids, for the first time we present the tidal love numbers at Next to Next to Leading order for a variety of dark matter admixed neutron stars in wEFT formalism. We show that loop corrections in the EFT to the TLN operator insertions leads to UV divergences which can be interpreted as the renormalization group evolution for this NNLO tidal love number. We show that its RG evolution has both a universal and non-universal term. The universal term can be inferred using the consistency of the EFT and we explicitly compute the non-universal term showing that it is proportional to the leading order TLN.

We note that the tidal Love number computed so far uses the near-far zone factorization framework which is ambiguous up to a universal constant term. To pin down this constant requires a full matching which is beyond the scope of this paper. Few recent papers [99, 100] have taken the first steps in this direction, performing a full matching to $O(\omega^3)$. However, for tidal love numbers we need a matching to at least $O(\omega^6)$, which will be a non trivial calculation and will be an interesting future work.

We have investigated the impact of increasing fraction of Dark Matter on the tidal deformability of the star. From the results for the fermionic Dark matter admixed neutron stars, we see that with increasing DM particle mass(M_{DM}) and DM mass fraction ($\%DM$), the allowable total mass of the NS drops significantly. The range of radii however is less affected, leading to a sizable decrease in compactness. In general, with increasing dark matter admixture, bosonic dark matter forms a larger halo around the neutron star. This reduces its compactness and we discuss in detail the impact on the TLNs in Section 5.

ρ_0	%DM	M	R (km)	R_{DM} (km)	C	k_2^e	$\nu_2^e(\times 10^3)$	κ_2^e
500	0	1.88	13.18	0	0.21	0.071	0.027	0.15
500	3.75	1.84	12.93	13.84	0.2	0.051	0.017	0.18
500	6.5	1.85	12.83	16.92	0.16	0.02	0.0049	0.25
500	13.04	1.94	12.7	23.38	0.12	0.0086	0.00067	0.31
500	19.05	2.05	12.63	28.52	0.11	0.01	0.0002	0.35
750	0	2.1	12.63	0	0.25	0.045	0.000018	0.13
750	3.7	2.05	12.39	12.82	0.24	0.038	0.014	0.13
750	10.57	2.11	12.17	19.77	0.16	0.0069	0.00094	0.24
750	18.32	2.26	12.06	26.54	0.13	0.0076	0.00016	0.3
750	32.94	2.69	11.93	34.42	0.12	0.021	0.000033	0.32
1000	0	2.15	12.12	0	0.26	0.034	0.015	0.12
1000	3.7	2.1	11.89	12.2	0.25	0.03	0.013	0.11
1000	6.51	2.11	11.78	15.08	0.21	0.011	0.0032	0.18
1000	11.74	2.18	11.66	20.15	0.16	0.0052	0.00053	0.24
1000	18.01	2.3	11.57	25.6	0.13	0.0067	0.00012	0.28
1000	27.67	2.56	11.48	32.02	0.12	0.013	0.000032	0.31

Table 2: Properties of stars composed of Bosonic DM ($A_\chi = 0.4 \frac{\text{m}^5}{\text{kg s}^2}$) mixed with FSU2 equation of state for non-viscous baryon matter. We consider three distinct central densities ρ_0 in units of $\frac{\text{MeV}}{\text{fm}^3}$ with increasing DM fraction.

There are various open questions to be explored following our work. Understanding the effect of dynamical TLN on GW waveform is of paramount importance. There are some recent studies on the feasibility of constraining NNLO TLN for BH and neutron stars in next generation GW detectors[32, 34, 57]. With the Wilson coefficients for the EFT operators in hand, we can apply this formalism to perform a full analysis for the binary system computing the impact of the TLNs on the Gravitational Wave spectrum. This will tell us which type of binary systems would be the most suitable candidates for phenomenological studies beyond the leading TLNs. This is an important part of our goal of improving the constraints on the microscopic structure of Neutron stars and the accreted Dark Matter halos. Understanding various EoS independent universality relations for dynamical TLN is also another important avenue to investigate in relation to GW astronomy.

Further, in our work we have restricted the calculation to non-rotating stars but most astrophysical Neutron stars have non zero spin. While the BHPT low frequency expansion for Kerr BHs has been recently worked out [1], the case for rotating stars with non-zero reflectivity is still an open problem and is a natural extension of our work. The non-trivial problem however, is solving for the stellar interior with only axial symmetry.

Finally, in this paper, we have only considered non viscous fluids due to the limitation of the hydrodynamical description. This can be remedied using various prescriptions such as the Israel-Stewart model and would be a natural extension of this work.

Acknowledgments

S.M. wants to thank Sumanta Chakraborty, Valerio De Luca, Jordan Wilson-Gerow for insightful discussions on various aspects of Love numbers and tidal dissipation. V.V. is supported by startup funds from the University of South Dakota and by the U.S. Department of Energy, EPSCoR program under contract No. DE-SC0025545.

Appendix

A MST method for scattering amplitude

In this appendix, we elaborate on the MST method used to obtain the scattering amplitude used in the main text. In a general rotating (Kerr) spacetime, the black hole perturbation theory is written in terms of *curvature* perturbation, with the help of Newman-Penrose tetrad formalism. The starting point in this case is the Weyl scalar $\Psi_4 = -C_{\alpha\beta\gamma\delta}\bar{m}^\alpha l^\beta \bar{m}^\gamma l^\delta$, where, Weyl tensor $C_{\alpha\beta\gamma\delta}$ is the Weyl tensor and $l^\alpha, n^\alpha, m^\alpha, \bar{m}^\alpha$ are the null tetrads. The Weyl scalar can then be decomposed into spheroidal harmonics, $\Psi_4 = e^{-i\omega t} e^{im\phi} S_\ell^m(\theta) R_{\omega\ell m}(r)$ where the angular part $S_\ell^m(\theta)$ and radial part $R_{\omega\ell m}(r)$ satisfies spheroidal harmonics differential equation and radial Teukolsky equation respectively (see eqn.(9) and (10) of [69]). On the other hand, in case of non-rotating BHs, perturbation theory can be written down in terms of *metric* perturbation quantities giving rise to Regge-Wheeler(RW)[71] and Zerilli equation [101]. Further, for compact objects surface reflectivity is defined through boundary conditions of RW variable, instead of radial Teukolsky variable which does not have a plane wave representation at the BH horizon. The two formalism however, is connected as it has been shown by Chandrasekhar [102] that radial Teukolsky equation can be transformed into RW equation in Schwarzschild limit. As in our case, we are only interested in solving non-rotating problem, we will therefore work with RW variable satisfying the equation,

$$\left[\frac{d^2}{dr_*^2} + (\omega^2 - V(r)) \right] X_{\omega\ell}(r) = 0 \quad (\text{A.1})$$

with,

$$V(r) = \left(1 - \frac{2M}{r} \right) \left[\frac{\ell(\ell+1)}{r^2} - \frac{6M}{r^3} \right] \quad (\text{A.2})$$

We will now use MST formalism outlined in [72] to solve the RW equation. In MST formalism, one introduces the renormalized angular momentum $\nu \sim \ell + \mathcal{O}(\omega^2)$, and solve the perturbation equation separately in near zone ($r_H \leq |r| < \infty$) and far zone ($r_H < |r| \leq \infty$), and then matching in the overlapping intermediate zone $r_H < |r| < \infty$.

In the near-zone, we make a change of variable to $x = \frac{r_H - r}{r_H}$, with the general solution of RW equation in this region can be written in terms of hypergeometric functions as,

$$X = \mathfrak{B}_\nu X_0^\nu(x) + \mathfrak{B}_{-\nu-1} X_0^{-\nu-1}(x) \quad (\text{A.3})$$

where, we have defined,

$$X_0^\nu(x) = N e^{i\epsilon x} (-x)^{-i\epsilon} \left[\sum_{n=-\infty}^{\infty} a_n^\nu (1-x)^{n+\nu+1+i\epsilon} \frac{\Gamma(a)\Gamma(b-a)}{\Gamma(c-a)} \right. \\ \left. {}_2F_1\left(a, c-b, a-b+1; \frac{1}{1-x}\right) \right] \quad (\text{A.4})$$

where, $\epsilon = 2GM\omega$, ${}_2F_1$ is the hypergeometric function and the arguments are given by, $a = -n - \nu + s - i\epsilon$, $b = n + \nu + s + 1 - i\epsilon$, $c = 1 - 2i\epsilon$.⁴ Further, $N = \frac{\Gamma(1-s-2i\epsilon)}{\Gamma(-\nu-i\epsilon)\Gamma(1+\nu-i\epsilon)}$ is a normalization constant. As in this work, we are interested in deriving only up to NNLO TLNs, we have to keep at least up to $\mathcal{O}(\omega^2)$ terms. The renormalised angular momentum ν and the coefficients a_n^ν up to this order is given in [72], and we have taken the same for our calculation in this paper. Finally the 'reflectivity' terms $\mathfrak{B}_{\nu, -\nu-1}$ needs to be fixed using boundary condition as shown in main text. In case of a BH, $\frac{\mathfrak{B}_{-\nu-1}}{\mathfrak{B}_\nu} = 1$.

Next we solve eqn. (A.1) at far zone $r_H < |r| \leq \infty$. In this limit we once again change the variable to $z = \omega r$. In this variable the general solution of RW equation is given in terms of coulomb functions X_C^ν , and $X_C^{-\nu-1}$, where,

$$X_C^\nu(z) = N_C^\nu e^{-iz} \left(1 - \frac{\bar{\omega}}{z}\right)^{-i\bar{\omega}} (-2iz)^{\nu+1} \sum_{n=-\infty}^{\infty} a_n^\nu \frac{\Gamma(n+\nu+1+s-i\bar{\omega})\Gamma(n+\nu+1-i\bar{\omega})}{\Gamma(n+\nu+1-s+i\bar{\omega})\Gamma(2n+2\nu+2)} \quad (\text{A.5}) \\ \times (2iz)^n M(n+\nu+1+i\bar{\omega}, 2n+2\nu+2, 2iz)$$

where, M is confluent hypergeometric function, and the normalisation constant N_C^ν is given by,

$$N_C^\nu = \frac{\Gamma(\nu+1-s+i\bar{\omega})\Gamma(\nu+1+i\bar{\omega})}{2\Gamma(\nu+1+s-i\bar{\omega})\Gamma(\nu+1-i\bar{\omega})} e^{i\frac{\pi}{2}(\nu+1)} \quad (\text{A.6})$$

In [68], the authors first noted that in the region where both the near zone solution X_0^ν and the far zone solution X_C^ν in convergent ($r_H < |r| < \infty$), satisfy the same analytic properties and therefore can be related to each other proportionally as

$$X_0^\nu = K_\nu X_C^\nu \quad (\text{A.7})$$

where

⁴In the expression (A.4), we have corrected a mistype in eqn. 3.23 of [72].

$$\begin{aligned}
K_\nu &= \frac{e^{i\epsilon}(2\epsilon)^{s-\nu}2^{-s}\Gamma(1-s-2i\epsilon)\Gamma(2\nu+2)}{\Gamma(\nu+1-s+i\epsilon)\Gamma(\nu+1+i\epsilon)\Gamma(\nu+1+s+i\epsilon)} \\
&\times \left(\sum_{n=0}^{\infty} \frac{\Gamma(n+2\nu+1)}{(n)!} \frac{\Gamma(n+\nu+1+s+i\epsilon)}{\Gamma(n+\nu+1-s-i\epsilon)} \frac{\Gamma(\nu+1+i\epsilon)}{\Gamma(\nu+1-i\epsilon)} a_n^\nu \right) \\
&\times \left(\sum_{n=-\infty}^0 \frac{1}{(-n)!(2\nu+2)_n} \frac{(\nu+1+s-i\epsilon)_n}{(\nu+1-s+i\epsilon)_n} \frac{(\nu+1-i\epsilon)_n}{(\nu+1+i\epsilon)_n} a_n^\nu \right)^{-1} \tag{A.8}
\end{aligned}$$

Finally, to obtain the scattering amplitude, we would need to connect the far zone solution to the boundary condition at infinity. For this purpose we need to write down $X_C^\nu(z)$ in terms of incoming and reflected wave at infinity, $X_C^\nu|_{r=z \rightarrow \infty} = A_{C,in}^\nu e^{-i\omega r^*} + A_{C,out}^\nu e^{i\omega r^*}$, with the explicit form of them given in eqn. 3.19 and eqn. 3.38 of [72]. Putting all of these ingredients together, one can obtain the scattering amplitude for the incident perturbation given by RW equation in MST formalism

$$S = \omega^{-2s} e^{-2i\epsilon \ln \epsilon} \frac{A_{C,out}^\nu}{A_{C,in}^\nu} \left[\frac{1 + \beta_\nu \frac{K_{-\nu-1}}{K_\nu} \left(\frac{\mathfrak{B}_{-\nu-1}}{\mathfrak{B}_\nu} \right)}{1 + \alpha_\nu \frac{K_{-\nu-1}}{K_\nu} \left(\frac{\mathfrak{B}_{-\nu-1}}{\mathfrak{B}_\nu} \right)} \right]. \tag{A.9}$$

where, $\alpha_\nu = -ie^{i\pi\nu} \frac{\sin(\nu-s+i\epsilon)}{\sin(\nu+s-i\epsilon)}$, $\beta_\nu = ie^{i\pi\nu}$.

B Additional results for TLNs

Here we present additional results for the fermionic DM admixed neutron stars.

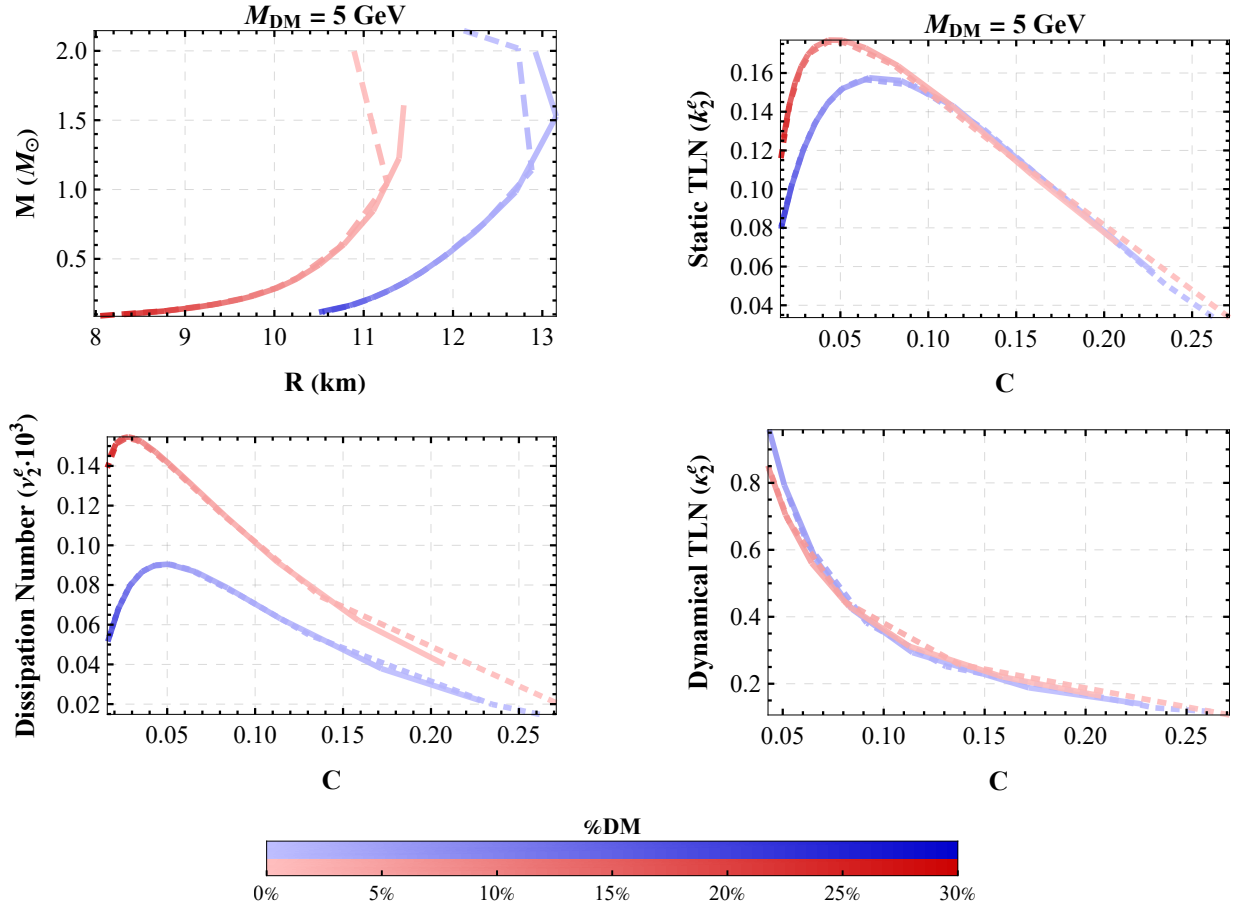


Figure 7: Mass-radius relationship for fermionic DM admixed neutron star. Two baryonic EoS, FSU2 and SFHO, are denoted with blue and red curves respectively. Each line progresses from light to darker shades, representing lower DM mass fraction (%DM) and higher DM mass fractions respectively. Solid and dashed lines represent central baryonic densities of 650 and $1000 \frac{\text{MeV}}{\text{fm}^3}$ respectively.

ρ_0	%DM	M	R (km)	R_{dm} (km)	C	k_2^e	$\nu_2^e (\times 10^3)$	κ_2^e
500	0.66	1.67	13.23	0.71	0.19	0.089	0.033	0.17
500	1.08	1.48	13.18	0.61	0.17	0.11	0.04	0.19
500	1.61	1.23	13.01	0.55	0.14	0.13	0.051	0.23
500	2.48	0.92	12.63	0.5	0.11	0.15	0.066	0.31
800	0.67	2.01	12.82	0.64	0.23	0.054	0.021	0.14
800	1.36	1.72	13.13	0.49	0.19	0.081	0.03	0.17
800	2.23	1.26	12.97	0.42	0.14	0.12	0.049	0.23
800	3.13	0.95	12.6	0.4	0.11	0.14	0.064	0.31
1500	0.79	2.12	11.9	0.57	0.26	0.031	0.014	0.12
1500	1.58	1.89	12.92	0.39	0.22	0.063	0.024	0.15
1500	2	1.6	13.09	0.35	0.18	0.091	0.034	0.18
1500	3.03	1.1	12.77	0.32	0.13	0.13	0.056	0.26

Table 3: 5 GeV fermionic matter with FSU2 equation of state with non-viscous baryon matter

References

- [1] M. V. S. Saketh, Z. Zhou, and M. M. Ivanov, *Phys. Rev. D* **109**, 064058 (2024), [arXiv:2307.10391 \[hep-th\]](#) .
- [2] M. V. S. Saketh, Z. Zhou, S. Ghosh, J. Steinhoff, and D. Chatterjee, *Phys. Rev. D* **110**, 103001 (2024), [arXiv:2407.08327 \[gr-qc\]](#) .
- [3] J. Aasi *et al.* (LIGO Scientific), *Class. Quant. Grav.* **32**, 074001 (2015), [arXiv:1411.4547 \[gr-qc\]](#) .
- [4] F. Acernese *et al.* (VIRGO), *Class. Quant. Grav.* **32**, 024001 (2015), [arXiv:1408.3978 \[gr-qc\]](#) .
- [5] T. Akutsu *et al.* (KAGRA), *PTEP* **2021**, 05A102 (2021), [arXiv:2009.09305 \[gr-qc\]](#) .
- [6] R. Abbott *et al.* (KAGRA, VIRGO, LIGO Scientific), *Phys. Rev. X* **13**, 041039 (2023), [arXiv:2111.03606 \[gr-qc\]](#) .
- [7] R. Abbott *et al.* (LIGO Scientific, VIRGO), *Phys. Rev. D* **109**, 022001 (2024), [arXiv:2108.01045 \[gr-qc\]](#) .
- [8] B. P. Abbott *et al.* (LIGO Scientific, Virgo), *Phys. Rev. Lett.* **116**, 061102 (2016), [arXiv:1602.03837 \[gr-qc\]](#) .
- [9] B. P. Abbott *et al.* (LIGO Scientific, Virgo), *Phys. Rev. Lett.* **116**, 221101 (2016), [Erratum: *Phys.Rev.Lett.* 121, 129902 (2018)], [arXiv:1602.03841 \[gr-qc\]](#) .
- [10] B. P. Abbott, R. Abbott, T. Abbott, F. Acernese, K. Ackley, C. Adams, T. Adams, P. Addesso, R. X. Adhikari, V. B. Adya, *et al.*, *Physical review letters* **121**, 161101 (2018).
- [11] S. Nissanke, D. E. Holz, N. Dalal, S. A. Hughes, J. L. Sievers, and C. M. Hirata, (2013), [arXiv:1307.2638 \[astro-ph.CO\]](#) .
- [12] B. P. Abbott *et al.* (LIGO Scientific, Virgo, 1M2H, Dark Energy Camera GW-E, DES, DLT40, Las Cumbres Observatory, VINROUGE, MASTER), *Nature* **551**, 85 (2017), [arXiv:1710.05835 \[astro-ph.CO\]](#) .
- [13] M. Maggiore *et al.* (ET), *JCAP* **03**, 050 (2020), [arXiv:1912.02622 \[astro-ph.CO\]](#) .
- [14] P. Amaro-Seoane, H. Audley, S. Babak, J. Baker, E. Barausse, P. Bender, E. Berti, P. Binetruy, M. Born, D. Bortoluzzi, *et al.*, *arXiv preprint arXiv:1702.00786* (2017).
- [15] K. G. Arun *et al.* (LISA), *Living Rev. Rel.* **25**, 4 (2022), [arXiv:2205.01597 \[gr-qc\]](#) .
- [16] C. Jockel and L. Sagunski, *Particles* **7**, 52 (2024), [arXiv:2310.17291 \[gr-qc\]](#) .
- [17] L. Cipriani, E. Giangrandi, V. Sagun, D. D. Doneva, and S. S. Yazadjiev, *Phys. Rev. D* **111**, 123005 (2025), [arXiv:2502.17948 \[astro-ph.HE\]](#) .
- [18] B. Kain, *Phys. Rev. D* **103**, 043009 (2021), [arXiv:2102.08257 \[gr-qc\]](#) .
- [19] J. Cronin, X. Zhang, and B. Kain, *Phys. Rev. D* **108**, 103016 (2023), [arXiv:2311.07714 \[gr-qc\]](#) .
- [20] R. M. Santos, R. C. Nunes, J. G. Coelho, and J. C. de Araujo, *arXiv preprint arXiv:2508.19382* (2025).
- [21] E. Poisson and C. M. Will, *Gravity: Newtonian, post-newtonian, relativistic* (Cambridge University Press, 2014).
- [22] A. Le Tiec and M. Casals, *Phys. Rev. Lett.* **126**, 131102 (2021), [arXiv:2007.00214 \[gr-qc\]](#) .
- [23] R. P. Bhatt, S. Chakraborty, and S. Bose, *Phys. Rev. D* **108**, 084013 (2023), [arXiv:2306.13627 \[gr-qc\]](#) .
- [24] H. S. Chia, *Phys. Rev. D* **104**, 024013 (2021), [arXiv:2010.07300 \[gr-qc\]](#) .
- [25] T. Hinderer, *Astrophys. J.* **677**, 1216 (2008), [Erratum: *Astrophys.J.* 697, 964 (2009)], [arXiv:0711.2420 \[astro-ph\]](#) .

- [26] H. Koehn, E. Giangrandi, N. Kunert, R. Somasundaram, V. Sagun, and T. Dietrich, *Phys. Rev. D* **110**, 103033 (2024), [arXiv:2408.14711 \[astro-ph.HE\]](#) .
- [27] R. F. Diedrichs, N. Becker, C. Jockel, J.-E. Christian, L. Sagunski, and J. Schaffner-Bielich, *Phys. Rev. D* **108**, 064009 (2023), [arXiv:2303.04089 \[gr-qc\]](#) .
- [28] D. Rafiei Karkevandi, S. Shakeri, V. Sagun, and O. Ivanytskyi, in *16th Marcel Grossmann Meeting on Recent Developments in Theoretical and Experimental General Relativity, Astrophysics and Relativistic Field Theories* (2021) [arXiv:2112.14231 \[astro-ph.HE\]](#) .
- [29] E. Giangrandi, V. Sagun, O. Ivanytskyi, C. Providência, and T. Dietrich, *Astrophys. J.* **953**, 115 (2023), [arXiv:2209.10905 \[astro-ph.HE\]](#) .
- [30] M. Mariani, C. Albertus, M. del Rosario Alessandroni, M. G. Orsaria, M. A. Perez-Garcia, and I. F. Ranea-Sandoval, *Mon. Not. Roy. Astron. Soc.* **527**, 6795 (2024), [arXiv:2311.14004 \[astro-ph.HE\]](#) .
- [31] S. Mukherjee, P. S. Aswathi, C. Singha, and A. Ganguly, (2025), [arXiv:2506.22353 \[gr-qc\]](#) .
- [32] J. A. Saes, A. Hegade K. R., and N. Yunes, (2025), [arXiv:2511.19626 \[gr-qc\]](#) .
- [33] S. Chakrabarti, T. Delsate, and J. Steinhoff, (2013), [arXiv:1304.2228 \[gr-qc\]](#) .
- [34] A. Hegade K. R., J. L. Ripley, and N. Yunes, *Phys. Rev. D* **109**, 104064 (2024), [arXiv:2403.03254 \[gr-qc\]](#) .
- [35] J. Steinhoff, T. Hinderer, A. Buonanno, and A. Taracchini, *Phys. Rev. D* **94**, 104028 (2016), [arXiv:1608.01907 \[gr-qc\]](#) .
- [36] T. Hinderer *et al.*, *Phys. Rev. Lett.* **116**, 181101 (2016), [arXiv:1602.00599 \[gr-qc\]](#) .
- [37] G. Pratten, P. Schmidt, and N. Williams, *Phys. Rev. Lett.* **129**, 081102 (2022), [arXiv:2109.07566 \[astro-ph.HE\]](#) .
- [38] L. Bildsten and C. Cutler, *Astrophysical Journal*, Part 1 (ISSN 0004-637X), vol. 400, no. 1, p. 175-180. **400**, 175 (1992).
- [39] J. L. Ripley, A. Hegade K. R., R. S. Chandramouli, and N. Yunes, *Nature Astron.* **8**, 1277 (2024), [arXiv:2312.11659 \[gr-qc\]](#) .
- [40] J. L. Ripley, A. Hegade K. R., and N. Yunes, *Phys. Rev. D* **108**, 103037 (2023), [arXiv:2306.15633 \[gr-qc\]](#) .
- [41] S. Chakraborty, E. Maggio, M. Silvestrini, and P. Pani, (2023), [arXiv:2310.06023 \[gr-qc\]](#) .
- [42] R. P. Bhatt, S. Chakraborty, and S. Bose, *Phys. Rev. D* **111**, L041504 (2025), [arXiv:2406.09543 \[gr-qc\]](#) .
- [43] V. De Luca and P. Pani, *JCAP* **08**, 032 (2021), [arXiv:2106.14428 \[gr-qc\]](#) .
- [44] V. De Luca, A. Maselli, and P. Pani, *Phys. Rev. D* **107**, 044058 (2023), [arXiv:2212.03343 \[gr-qc\]](#) .
- [45] R. Brito and S. Shah, *Phys. Rev. D* **108**, 084019 (2023), [arXiv:2307.16093 \[gr-qc\]](#) .
- [46] K. Chakravarti, S. Chakraborty, S. Bose, and S. SenGupta, *Phys. Rev. D* **99**, 024036 (2019), [arXiv:1811.11364 \[gr-qc\]](#) .
- [47] D. Pereñiguez and V. Cardoso, *Phys. Rev. D* **105**, 044026 (2022), [arXiv:2112.08400 \[gr-qc\]](#) .
- [48] R. Dey, S. Biswas, and S. Chakraborty, *Phys. Rev. D* **103**, 084019 (2021), [arXiv:2010.07966 \[gr-qc\]](#) .
- [49] V. Cardoso, E. Franzin, A. Maselli, P. Pani, and G. Raposo, *Phys. Rev. D* **95**, 084014 (2017), [Addendum: *Phys.Rev.D* 95, 089901 (2017)], [arXiv:1701.01116 \[gr-qc\]](#) .
- [50] S. Nair, S. Chakraborty, and S. Sarkar, *Phys. Rev. D* **109**, 064025 (2024), [arXiv:2401.06467 \[gr-qc\]](#) .

- [51] S. Barbosa, P. Brax, S. Fichet, and L. de Souza, *JCAP* **07**, 071 (2025), [arXiv:2501.18684 \[hep-th\]](#) .
- [52] E. Franzin, A. M. Frassino, and J. V. Rocha, *JHEP* **12**, 224 (2025), [arXiv:2410.23545 \[hep-th\]](#) .
- [53] S. Datta, R. Brito, S. A. Hughes, T. Klinger, and P. Pani, (2024), [arXiv:2404.04013 \[gr-qc\]](#) .
- [54] S. Datta, R. Brito, S. Bose, P. Pani, and S. A. Hughes, *Phys. Rev. D* **101**, 044004 (2020), [arXiv:1910.07841 \[gr-qc\]](#) .
- [55] A. Maselli, P. Pani, V. Cardoso, T. Abdelsalhin, L. Gualtieri, and V. Ferrari, *Phys. Rev. Lett.* **120**, 081101 (2018), [arXiv:1703.10612 \[gr-qc\]](#) .
- [56] S. Nair, S. Chakraborty, and S. Sarkar, *Phys. Rev. D* **107**, 124041 (2023), [arXiv:2208.06235 \[gr-qc\]](#) .
- [57] S. Chakraborty, V. De Luca, L. Gualtieri, and P. Pani, *Phys. Rev. D* **112**, 104015 (2025), [arXiv:2507.22994 \[gr-qc\]](#) .
- [58] B. Kol and M. Smolkin, *JHEP* **02**, 010 (2012), [arXiv:1110.3764 \[hep-th\]](#) .
- [59] T. Katagiri, K. Yagi, and V. Cardoso, *Phys. Rev. D* **111**, 084080 (2025), [arXiv:2409.18034 \[gr-qc\]](#) .
- [60] W. D. Goldberger and I. Z. Rothstein, *Phys. Rev. D* **73**, 104029 (2006), [arXiv:hep-th/0409156](#) .
- [61] W. D. Goldberger and I. Z. Rothstein, *Gen. Rel. Grav.* **38**, 1537 (2006), [arXiv:hep-th/0605238](#) .
- [62] R. A. Porto, *Phys. Rept.* **633**, 1 (2016), [arXiv:1601.04914 \[hep-th\]](#) .
- [63] M. M. Ivanov and Z. Zhou, *Phys. Rev. D* **107**, 084030 (2023), [arXiv:2208.08459 \[hep-th\]](#) .
- [64] W. D. Goldberger and A. Ross, *Phys. Rev. D* **81**, 124015 (2010), [arXiv:0912.4254 \[gr-qc\]](#) .
- [65] R. A. Porto, A. Ross, and I. Z. Rothstein, *JCAP* **09**, 028 (2012), [arXiv:1203.2962 \[gr-qc\]](#) .
- [66] J. A. Futterman, F. Handler, and R. A. Matzner, (1987).
- [67] S. Mano, H. Suzuki, and E. Takasugi, *Prog. Theor. Phys.* **95**, 1079 (1996), [arXiv:gr-qc/9603020](#) .
- [68] S. Mano and E. Takasugi, *Prog. Theor. Phys.* **97**, 213 (1997), [arXiv:gr-qc/9611014](#) .
- [69] M. Sasaki and H. Tagoshi, *Living Rev. Rel.* **6**, 6 (2003), [arXiv:gr-qc/0306120](#) .
- [70] S. Mano, H. Suzuki, and E. Takasugi, *Prog. Theor. Phys.* **96**, 549 (1996), [arXiv:gr-qc/9605057](#) .
- [71] T. Regge and J. A. Wheeler, *Physical Review* **108**, 1063 (1957).
- [72] M. Casals and A. C. Ottewill, *Phys. Rev. D* **92**, 124055 (2015), [arXiv:1509.04702 \[gr-qc\]](#) .
- [73] J. Abedi, N. Afshordi, N. Oshita, and Q. Wang, *Universe* **6**, 43 (2020), [arXiv:2001.09553 \[gr-qc\]](#) .
- [74] K. Chakravarti, R. Ghosh, and S. Sarkar, *Phys. Rev. D* **109**, 046001 (2024), [arXiv:2310.18022 \[gr-qc\]](#) .
- [75] S. Datta and K. S. Phukon, *Phys. Rev. D* **104**, 124062 (2021), [arXiv:2105.11140 \[gr-qc\]](#) .
- [76] M. M. Ivanov and Z. Zhou, *Phys. Rev. Lett.* **130**, 091403 (2023), [arXiv:2209.14324 \[hep-th\]](#) .
- [77] Y. F. Bautista, G. Bonelli, C. Iossa, A. Tanzini, and Z. Zhou, *Phys. Rev. D* **109**, 084071 (2024), [arXiv:2312.05965 \[hep-th\]](#) .
- [78] L. D. Landau and E. M. Lifshitz, *Fluid Mechanics*, 2nd ed., Course of Theoretical Physics, Vol. 6 (Butterworth-Heinemann, Oxford, 1987).
- [79] J. R. Oppenheimer and G. M. Volkoff, *Phys. Rev.* **55**, 374 (1939).
- [80] L. Lindblom and S. L. Detweiler, *Astrophys. J. Suppl.* **53**, 73 (1983).
- [81] K. S. Thorne and A. Campolattaro, *Astrophys. J.* **149**, 591 (1967).
- [82] S. Ghosh, B. K. Pradhan, and D. Chatterjee, *Phys. Rev. D* **109**, 103036 (2024), [arXiv:2306.14737 \[gr-qc\]](#) .

- [83] C. S. Kochanek, *Astrophys. J.* **398**, 234 (1992).
- [84] Y. Kojima, *Phys. Rev. D* **46**, 4289 (1992).
- [85] S. Typel, M. Oertel, and T. Klähn, *Phys. Part. Nucl.* **46**, 633 (2015), [arXiv:1307.5715 \[astro-ph.SR\]](#) .
- [86] P. S. Shternin and D. G. Yakovlev, *Phys. Rev. D* **78**, 063006 (2008), [arXiv:0808.2018 \[astro-ph\]](#) .
- [87] C. Cutler and L. Lindblom, *Astrophys. J.* **314**, 234 (1987).
- [88] C. R. Argüelles, E. A. Becerra-Vergara, J. A. Rueda, and R. Ruffini, *Universe* **9**, 197 (2023), [arXiv:2304.06329 \[astro-ph.GA\]](#) .
- [89] S. Profumo, L. Giani, and O. F. Piattella, *Universe* **5**, 213 (2019), [arXiv:1910.05610 \[hep-ph\]](#) .
- [90] K.-L. Leung, M.-c. Chu, and L.-M. Lin, *Phys. Rev. D* **105**, 123010 (2022), [arXiv:2207.02433 \[astro-ph.HE\]](#) .
- [91] J. R. Oppenheimer and H. Snyder, *Phys. Rev.* **56**, 455 (1939).
- [92] T. Cohen, D. J. Phalen, A. Pierce, and K. M. Zurek, *Phys. Rev. D* **82**, 056001 (2010), [arXiv:1005.1655 \[hep-ph\]](#) .
- [93] J. Ellis, G. Hütsi, K. Kannike, L. Marzola, M. Raidal, and V. Vaskonen, *Phys. Rev. D* **97**, 123007 (2018), [arXiv:1804.01418 \[astro-ph.CO\]](#) .
- [94] M. F. Barbat, J. Schaffner-Bielich, and L. Tolos, *Phys. Rev. D* **110**, 023013 (2024), [arXiv:2404.12875 \[astro-ph.HE\]](#) .
- [95] E. G. M. Ferreira, *Astron. Astrophys. Rev.* **29**, 7 (2021), [arXiv:2005.03254 \[astro-ph.CO\]](#) .
- [96] E. G. M. Ferreira, *Astron. Astrophys. Rev.* **29**, 7 (2021), [arXiv:2005.03254 \[astro-ph.CO\]](#) .
- [97] Z. Buras-Stubbs and I. Lopes, *Phys. Rev. D* **109**, 043043 (2024).
- [98] C. G. Boehmer and T. Harko, *JCAP* **06**, 025 (2007), [arXiv:0705.4158 \[astro-ph\]](#) .
- [99] M. M. Ivanov, Y.-Z. Li, J. Parra-Martinez, and Z. Zhou, (2026), [arXiv:2602.06951 \[hep-th\]](#) .
- [100] Y. F. Bautista, M. Driesse, K. Haddad, and G. U. Jakobsen, (2026), [arXiv:2602.06125 \[hep-th\]](#) .
- [101] F. J. Zerilli, *Phys. Rev. Lett.* **24**, 737 (1970).
- [102] S. Chandrasekhar, *Proc. Roy. Soc. Lond. A* **343**, 289 (1975).